INTERNATIONAL ATOMIC ENERGY AGENCY
UNITED NATIONS EDUCATIONAL, SCIENTIFIC AND CULTURAL ORGANIZATION

INTERNATIONAL CENTRE FOR THEORETICAL PHYSICS
34100 TRIESTE (ITALY) - P.O.B. 586 - MIRAMARE - STRADA COSTIERA 11 - TELEPHONE: 2240-1
CABLE: CENTRATOM - TELEX 460392 - I

SMR/208 - 33

SPRING COLLEGE IN MATERIALS SCIENCE

ON

"METALLIC MATERIALS"

(11 May - 19 June 1987)

ORDERED INTERMETALLICS AND NICKEL-BASE SUPERALLOYS
(Part II)

C.T. LIU
Metals and Ceramics Division
Oak Ridge National Laboratory
Oak Ridge, Tennessee 37831-6117
U.S.A.

Ni-BASE SUPERALLOYS

1. HISTORICAL DEVELOPMENT OF Ni-BASE SUPERALLOYS
2. THE GIBBs PHASE RULE
3. EQUILIBRIUM PHASE DIAGRAMS OF BINARY AND TERNARY ALLOY SYSTEMS
4. BASIC ALLOY SYSTEMS

   Ni-Cr
   Ni-Al
   Ni-Cr-Al
5. COMPLEX NICKEL-BASE SUPERALLOYS: PHYSICAL METALLURGY AND ALLOY DESIGN

Ni-BASE SUPERALLOYS

- THE Ni-BASE SUPERALLOYS ARE THE MOST COMPLEX IN COMPOSITION AND MICROSTRUCTURES AND IN MANY RESPECTS THE MOST SUCCESSFUL HT ALLOYS IN CURRENT USE.
- THEIR DEVELOPMENT COMMENCED IN THE LATE 1930s WITH THE NEED FOR AIRCRAFT GAS-TURBINE COMPONENTS MATERIALS STRONGER THAN THE THEN-AVAILABLE AUSTENITIC STAINLESS STEELS.
- THE MAJOR APPLICATIONS OF Ni-BASE SUPERALLOYS ARE AS BLADES, DISKS, AND SHEET METAL PARTS OF GAS TURBINES. TYPICAL GAS-TURBINE ENGINES PRODUCED IN U.S. DURING THE 1970s UTILIZED Ni AND Co-BASE SUPERALLOYS FOR 55–60% OF TOTAL ENGINE WEIGHT.

DEVELOPMENT OF WROUGHT Ni-BASE SUPERALLOYS

- THE EARLIEST SUPERALLOYS WERE WROUGHT, I.E. THEY ARE FABRICATED TO FINAL SIZE BY A MECHANICAL WORKING OPERATION.
- IN ENGLAND, THE EARLIEST SUPERALLOY WAS NIMONIC 75, PRODUCED BY ADDING 0.3% Ti AND 0.1% C TO AN OXIDATION – RESISTANT SOLID SOLUTION 80% Ni–20% Cr (NICHROME) BASE.
- HIGHER ENGINE SPEEDS AND TURBINE INLET TEMPERATURE SPURRED SUCCEEDING MODIFICATION OF THIS ALLOY IN THE NIMONIC SERIES,
  - FIRST BY ADDING Al AND Ti TO PRODUCE γ' STRENGTHENING, AND
  - LATER BY ADDING Co TO RAISE THE VOLUME FRACTION OF γ' AND TO IMPROVE WORKABILITY (NIMONIC 90).
  - LATER ALLOYS IN THE NIMONIC SERIES HAVE INCORPORATED HIGHER Al PLUS Ti CONTENTS, AS WELL AS Mo FOR SS STRENGTHENING (NIMONICS 115 AND 120).
- THE COMPOSITIONS OF WROUGHT Ni-BASE SUPERALLOYS ARE LISTED IN THE TABLE 4.
- IN THE U.S., A SERIES OF Ni-Cr-Fe ALLOYS BASED ON THE SS INCONEL 600 ALLOY WERE DEVELOPMENT.
  - INITIALLY, THOSE DEPENDED UPON Al AND Ti FOR γ' STRENGTHENING.
  - TO THIS WAS ADDED 1% Nb TO FORM THE WELL-KNOWN INCONEL X-750 ALLOY.

Table 4. Compositions of Wrought Nickel-Base Superalloys, wt %

Alloy designation	Ni	Cr	Co	Mo	W	Al	Ti	Fe	Mn	Si	C	B	Other
Nickel-base													
Astroloy	55.1	15.0	17.0	5.25		4.0	3.5				0.06	0.030	
Inconel alloy 600	76.6	15.8						7.2	0.20	0.20	0.04		
Inconel alloy 601	60.7	23.0				1.35		14.1	0.50	0.25	0.05		
Inconel alloy 625	61.1	22.0		9.0		0.2	0.2	3.0	0.15	0.30	0.05		4.0Nb
Inconel alloy X-750	73.0	15.0				0.8	2.5	6.8	0.70	0.30	0.04		0.9Nb
IN-102	67.9	15.0		3.0	3.0	0.4	0.6	7.0			0.06	0.005	3.0Nb, 0.03Zr, 0.02Mg
IN-587	47.2	28.5	20.0			1.2	2.3				0.05	0.003	0.7Nb, 0.05Zr
IN-597	48.4	24.5	20.0	1.5		1.5	3.0				0.05	0.012	0.05Zr, 0.02Mg, 1.0Nb
IN-853	74.6	20.0				1.5	2.5				0.05	0.007	0.07Zr, 1.3Y_2O_3
M-252	55.2	20.0	10.0	10.0		1.0	2.6		0.50	0.50	0.15	0.005	
Nimonic alloy 80A	74.7	19.5	1.1			1.3	2.5		0.10	0.70	0.06		
Nimonic alloy 90	57.4	19.5	18.0			1.4	2.4		0.50	0.70	0.07		
Nimonic alloy 105	53.3	14.5	20.0	5.0		1.2	4.5		0.50	0.70	0.20		
Nimonic alloy 115	57.3	15.0	15.0	3.5		5.0	4.0				0.15		
Nimonic alloy PK.33	55.9	18.5	14.0	7.0		2.0	2.0	0.25	0.10	0.15	0.05	0.030	
Nimonic alloy 120	63.8	12.5	10.0	5.7		4.5	3.5				0.04		
Nimonic alloy 942	49.5	12.5	1.0	6.0		0.6	3.9	27.5			0.03		
RA-33	45.0	25.5	3.0	3.0	3.0			18.0	1.50	1.20	0.06		
René 41	55.3	19.0	11.0	10.0		1.5	3.1				0.09	0.005	
René 95	61.3	14.0	8.0	3.5	3.5	3.5	2.5				0.15	0.010	3.5Ta, 0.05Zr
TD Nickel	98.0												2.0ThO_2
TD NiC	78.0	20.0											2.0ThO_2
Udimet 500	53.6	18.0	18.5	4.0		2.9	2.9				0.08	0.006	0.05Zr
Udimet 520	56.9	19.0	12.0	6.0	1.0	2.0	310				0.08	0.005	
Udimet 700	53.4	15.0	18.5	5.2		4.3	3.5				0.08	0.030	
Udimet 710	54.9	18.0	15.0	3.0	1.5	2.5	5.0				0.07	0.020	
Unitemp AF2-1DA	59.5	12.0	10.0	3.0	6.0	4.6	3.0				0.32	0.015	1.5Ta, 0.10Zr
Waspaloy	58.3	19.5	13.5	4.3		1.3	3.0				0.08	0.006	0.06Zr

Table 4

- OTHER EARLY WROUGHT ALLOYS DEVELOPED IN U.S. INCLUDED WASPALOY AND M-252, WITH Mo FOR SS STRENGTHENING AND CARBIDE FORMATION IN ADDITION TO THE γ' STRENGTHENING PRODUCED BY Al AND Ti.
- VACUUM-ARC MELTING WAS INTRODUCED TO AVOID THE LOSS OF Ti AND Al BY OXIDATION AND TO KEEP GASEOUS ELEMENT CONTAMINATIONS DOWN TO ACCEPTABLE LEVELS.
- BY USING VAM, STRONGER WROUGHT ALLOYS, INCLUDING UDIMET 500 AND 700, AND RENÉ 41, ALL STRENGTHENED PRINCIPALLY BY γ', BECOME COMMERCIAL.
- HASTELLOY X, A SS AND CARBIDE-STRENGTHENED ALLOY, IS USED IN SHEET FORM FOR LESS HIGHLY STRESSED PARTS REQUIRING OXIDATION RESISTANCE.

DEVELOPMENT OF CAST Ni-BASE ALLOYS

- BY THE LATE 1950s, THE TEMPERATURE REQUIREMENTS OF ADVANCED ENGINES HAD OUT-STRIPPED THE CAPABILITIES OF THE EXISTING WROUGHT ALLOYS. THE NEW ALLOYS WITH ADEQUATE STRENGTH THAT WERE DEVELOPED COULD ONLY BE PROCESSED BY THE INVESTMENT CASTING PROCESS.
- AMONG THE MOST NOTABLE OF THESE VERY STRONG ALLOYS DEVELOPED IN THE 1960s WERE INCONEL 713 AND A LOW-CARBON VERSION, 713LC, AS WELL AS IN-100, B-1900, AND MAR-M-200 (SEE TABLE 5).
- IN GENERAL, THE CAST ALLOYS TENDED TO REPLACE PART OF THE Cr, WITH Mo, W, AND Ta, AND RETAIN HIGH VOLUME FRACTIONS (TO 60 WT %) OF γ'.
- THE USSR HAS DEVELOPED ALLOYS (E.G. ZH56-K) WITH STRENGTHS EQUIVALENT TO IN-100 AND MAR-M-200.
- IN ADDITION TO HIGHER STRENGTH, THE INVESTMENT CASTING PROCESS HAS GIVEN DESIGN FLEXIBILITY THAT HAS LED TO MANY FURTHER ADVANCES THROUGH AIR COOLING OF TURBINE COMPONENTS.

Table 5. Compositions of Cast Nickel-Base Superalloys, wt %

Alloy designation	Ni	Cr	Co	Mo	W	Ta	Nb	Al	Ti	C	B	Zr	Other
Nickel-base													
Alloy 713C	74	12.5		4.2			2.0	6.1	0.8	0.12	0.012	0.10	
B-1900	64	8.0	10.0	6.0		4.0		6.0	1.0	0.10	0.015	0.10	
IN-100/René 100	60	10/9.5	15.0	3.0				5.5	4.7/4.2	0.18	0.014	0.06	1.0V
IN-162	73	10.0		4.0	2.0	2.0	1.0	6.5	1.0	0.12	0.020	0.10	
IN-731	67	9.5	10.0	2.5				5.5	4.6	0.18	0.015	0.06	
IN-738	61	16.0	8.5	1.7	2.6	1.7	0.9	3.4	3.4	0.17	0.010	0.10	
IN-792	61	12.4	9.0	1.9	3.8	3.9		3.1	4.5	0.12	0.020	0.10	
Mar-M 200	60	9.0	10.0		12.0		1.0	5.0	2.0	0.15	0.015	0.05	
Mar-M 200 (DS)	60	9.0	10.0		12.0		1.0	5.0	2.0	0.13	0.015	0.05	
Mar-M 246	60	9.0	10.0	2.5	10.0	1.5		5.5	1.5	0.15	0.015	0.05	
Mar-M 421	61	15.8	9.5	2.0	3.8		2.0	4.3	1.8	0.15	0.015	0.05	
Mar-M 432	50	15.5	20.0		3.0	2.0	2.0	2.8	4.3	0.15	0.015	0.05	
NX188 (DS)	74			18.0				8.0		0.04			
René 77	58	14.6	15.0	4.2				4.3	3.3	0.07	0.016	0.04	
René 80	60	14.0	9.5	4.0	4.0			3.0	5.0	0.17	0.015	0.03	
TAZ-8A	68	6.0		4.0	4.0	8.0	2.5	6.0		0.12	0.004	1.00	
TRW-NASA VIA	61	6.1	7.5	2.0	5.8	9.0	0.5	5.4	1.0	0.13	0.020	0.13	0.5Re, 0.4Hf
Udimet 500	52	18.0	19.0	4.2				3.0	3.0	0.07	0.007	0.05	
WAZ-20 (DS)	72				20.0			6.5		0.20		1.50	
IN-939	48	22.5	19.0		2.0	1.4	1.0	1.9	3.7		0.010		

Table 5

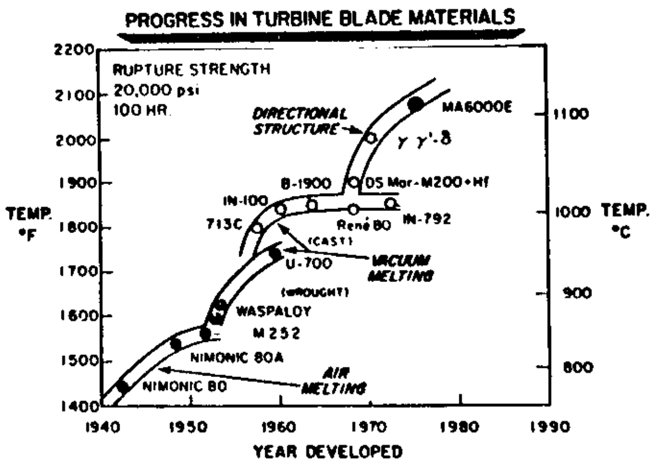

Progress in the Temperature Capability of Superalloys in the Last 40 Years

Fig. 3

MICROSTRUCTURE OF A NICKEL-BASE SUPERALLOY

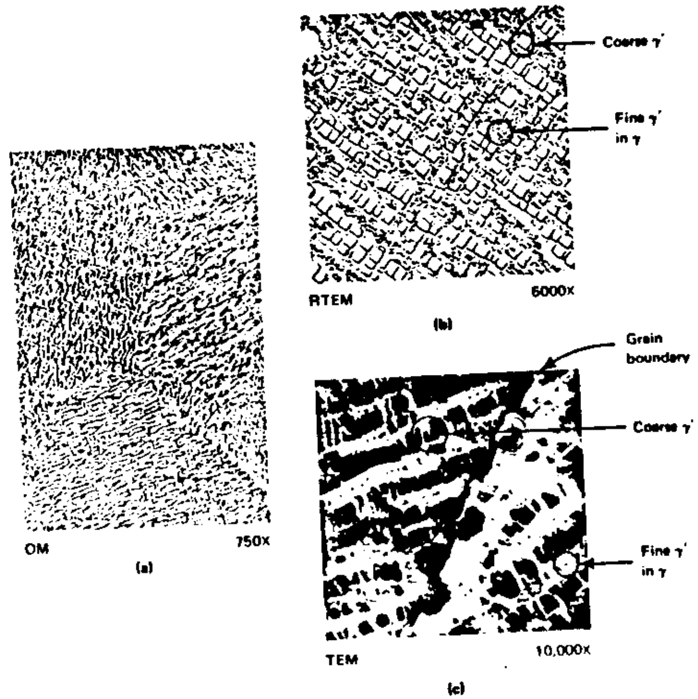

Fig. 5-1. Microstructure typical of Nimonic 115, heated for 1.5 h at 1190 °C, air cooled to 1100 °C, held 6 h, air cooled to 25 °C. This alloy contains approximately (wt %) 15Cr-5Al-4Ti-15Co-4Mo-0.18B-0.16C. (Adapted from C.H. White, in The Nimonic Alloys, 2d Ed., ed. W. Betteridge and J. Heslop, Edward Arnold Ltd, London, 1974)

DERIVATION OF GIBBs PHASE RULE

1. TOTAL NUMBER OF VARIABLES, V_1

   P = NUMBER OF PHASES

   C = NUMBER OF COMPONENTS

$$V_1 = \underbrace{P}_{\text{FOR PRESSURE VARIABLES}} + \underbrace{P}_{\text{FOR TEMPERATURE VARIABLES}} + \underbrace{P(C-1)}_{\text{FOR CONCENTRATION VARIABLES}}$$

$$= P(C+1)$$

2. TOTAL NUMBER OF CONSTRAINTS FOR AN EQUILIBRIUM CONDITION, V_2

$$V_2 = \underbrace{(P-1)}_{\text{FOR THE SAME PRESSURE}} + \underbrace{(P-1)}_{\text{FOR THE SAME TEMPERATURE}} + \underbrace{(P-1)C}_{\text{FOR THE SAME ACTIVITY OF EACH COMPONENT}}$$

$$= (P-1)(C+2)$$

3. INDEPENDENT VARIABLES OR DEGREES OF FREEDOM, V

$$V = V_1 - V_2 = P(C+1) - (P-1)(C+2) = C+2 - P$$

$\boxed{V = C+2 - P}$ ← THE GIBBs PHASE RULE.

BINARY ALLOY PHASE DIAGRAMS

$$V = C + 1 - P$$

FOR C = 2 $\quad V = 3 - P$

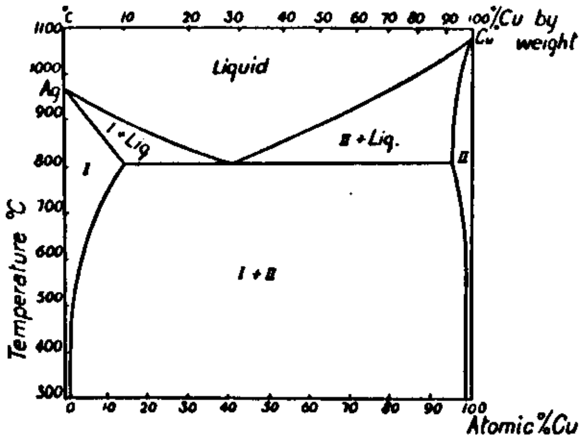

FIG. 79.—The Equilibrium Diagram of the Silver-Copper System.

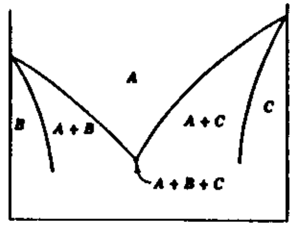

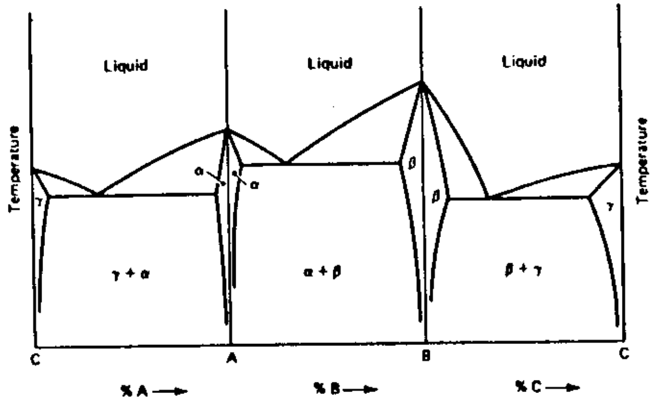

Fig. 4-1. Three eutectic binary phase diagrams of the systems A-B, B-C and C-A.

$V = C+1-P$

FOR $C=3$

$V = 4-P$

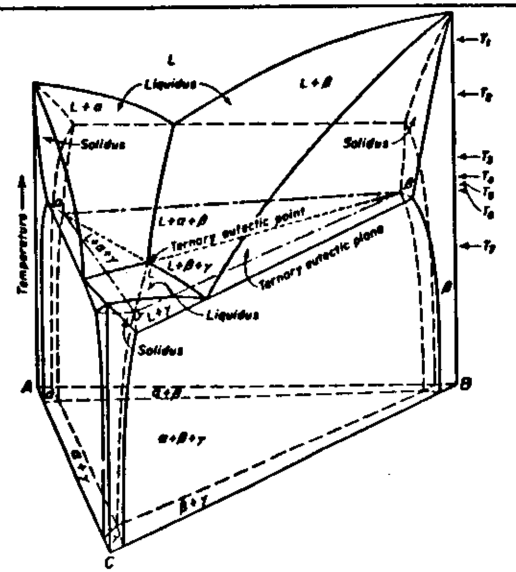

Fig. 4-2. Assumed ternary diagram for the system A-B-C. (From Phase Diagrams in Metallurgy, by F. N. Rhines. Copyright © 1956, McGraw-Hill, New York. Used with the permission of McGraw-Hill Book Company)

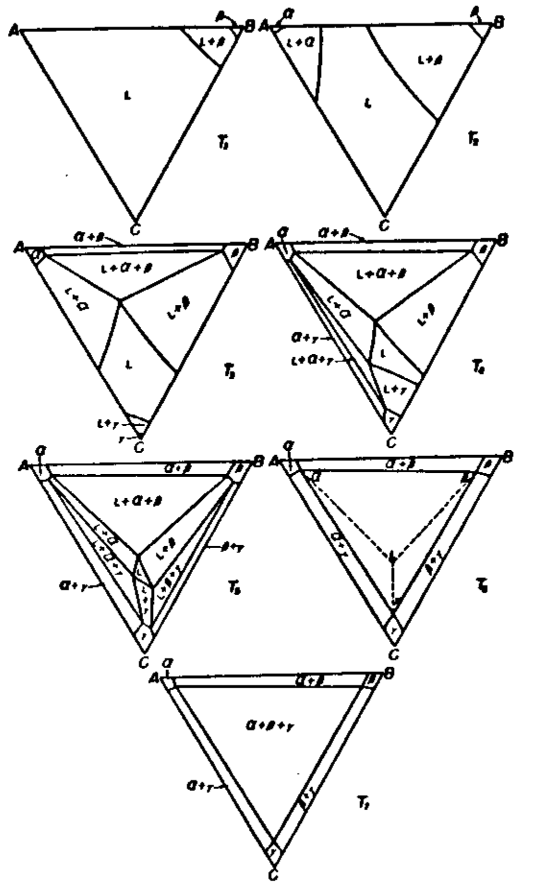

Fig. 4-3. Isothermal sections from the ternary A-B-C phase diagram, at the temperatures indicated in Fig. 4-2. (From same source as Fig. 4-2; used with the permission of McGraw-Hill Book Company)

$V = 3-P$

TERNARY PHASE DIAGRAMS

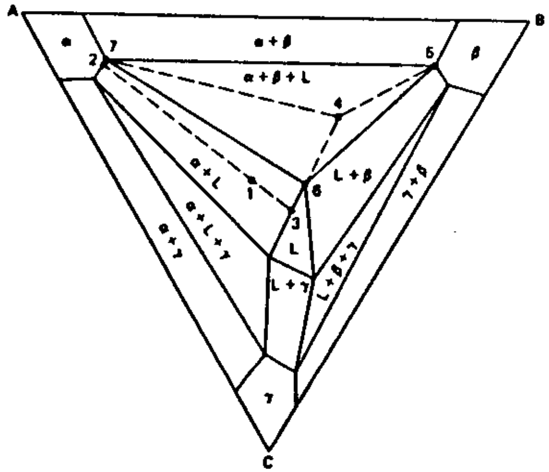

Fig. 4-4. Isothermal section at temperature T_s, used to illustrate the chemical composition of the phases in a two-phase and three-phase region.

$V = 3-P$

BASIC ALLOY SYSTEMS

(A) THE Ni-Cr SYSTEM: OXIDATION RESISTANCE

- THE Ni-Cr PHASE DIAGRAM
- OXIDATION MECHANISM
- KINETICS: $DM/DT = KT^{-1/2}$ $(\Delta M)^2 = K_pT$
- FORMATION OF DENSE AND ADHERENT OXIDE
- >20% Cr FOR GOOD OXIDATION RESISTANCE AT HIGH TEMPERATURES

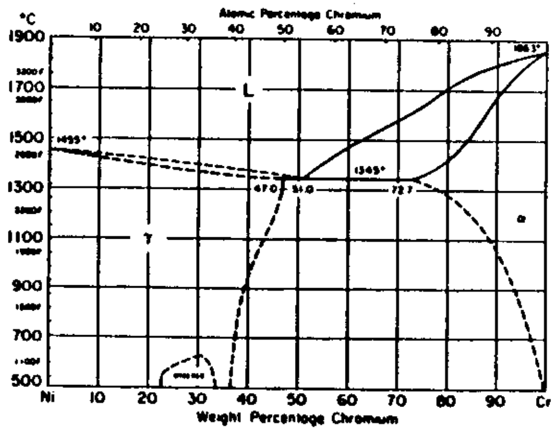

Fig. 5-4. The Ni-Cr phase diagram. The ordered structure occurs at Ni_2Cr, but its formation rate is very low. (From Metals Handbook, 8th Ed., Vol 8, American Society for Metals, Metals Park, Ohio, 1973)

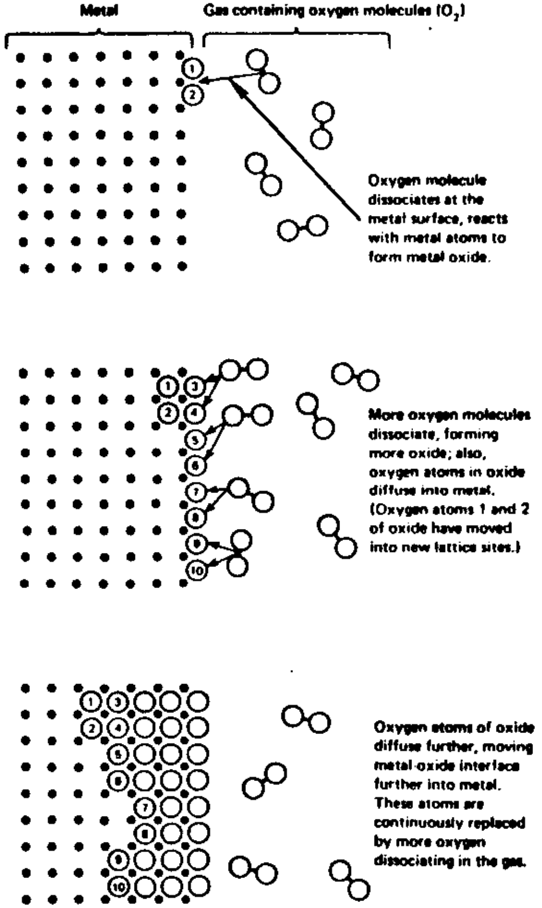

Fig. 5-2. Schematic illustration of a possible mechanism of oxidation of a metal.

same behavior, where thermodynamically Cr_2O_3 is stable, but the rate of formation is sufficiently low that they can be used in many high-temperature oxidizing conditions.

Another important consideration is the adherence of the protective oxide film during thermal cycling. The underlying metal and the oxide have differ-

(B) THE Ni-Al SYSTEM: PRECIPITATION HARDENING

- THE PHASE DIAGRAM AND PRECIPITATION OF γ' PHASE
- LATTICE STRUCTURE OF γ AND γ'
- SCHEMATIC ILLUSTRATION OF LATTICE STRAIN IN γ MATRIX DUE TO MISMATCH BETWEEN γ AND γ'
- AGE HARDENING
  - HARDENING IS DUE TO ELASTIC INTERFACE STRAINS WHICH IMPEDE THE DISLOCATION MOTION
  - OVER-AGING IS DUE TO A COARSENING OF γ' PARTICLES

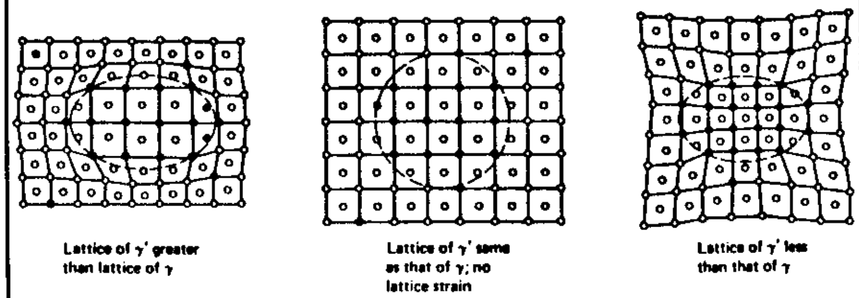

Fig. 5-11. Schematic illustration of lattice strain in γ matrix due to lattice mismatch between γ' and γ. (Adapted from H. Warlimont, in Electron Microscopy and Structure of Materials, ed. G. Thomas, University of California Press, Los Angeles, 1971)

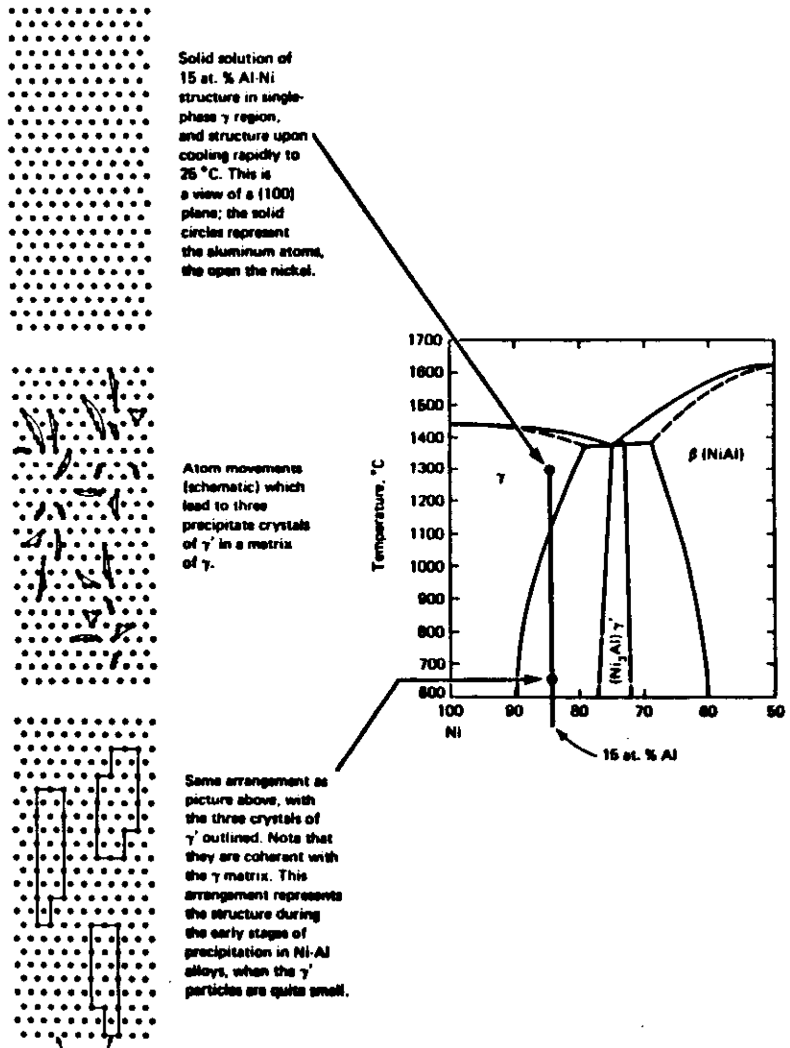

Fig. 5-8. Schematic arrangement of the precipitation of γ' crystals from γ in a Ni-Al alloy containing 15 at.% Al. The atom movements show possible atom shifts to create the three crystals of γ'. (The exact mechanism would involve vacancy movement, not depicted here.)

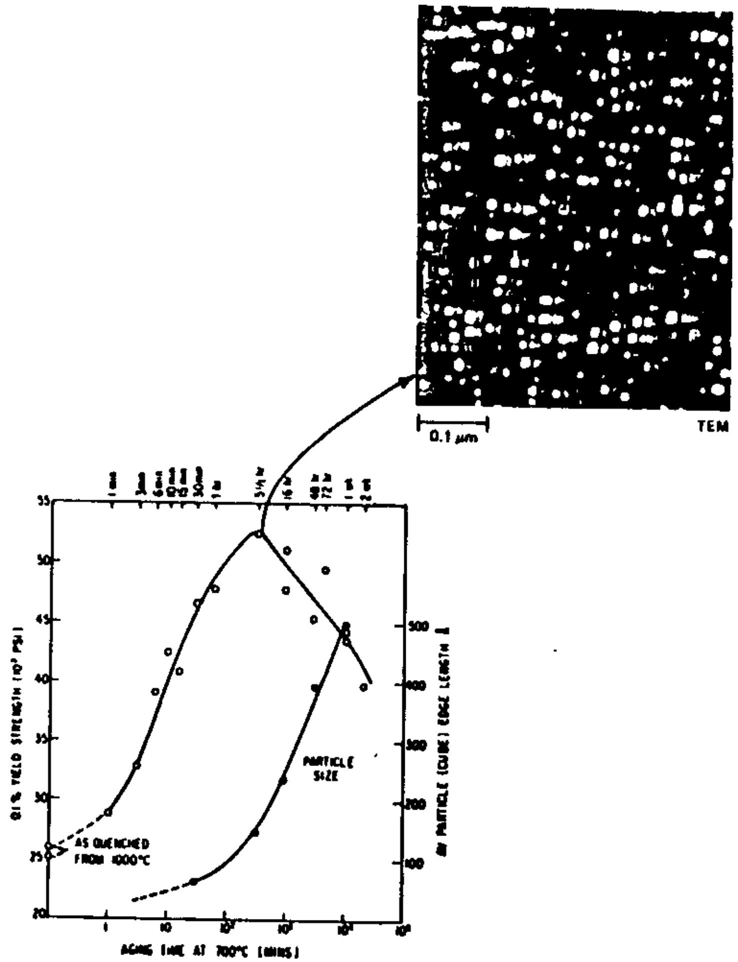

Fig. 5-9. Effect of aging time at 700 °C on the yield strength (at 25 °C) and γ' particle size of a Ni – 12.7 at.% Al alloy. The microstructure (dark-field electron micrograph) shows the cuboidal γ' particles in the γ matrix. (Adapted from V. A. Phillips, Acta Met., Vol 14, p 1535, 1966)

(C) THE Ni-Cr-Al SYSTEM

- THE TERNARY PHASE DIAGRAM
- GOOD HIGH-TEMPERATURE AND OXIDATION RESISTANCE

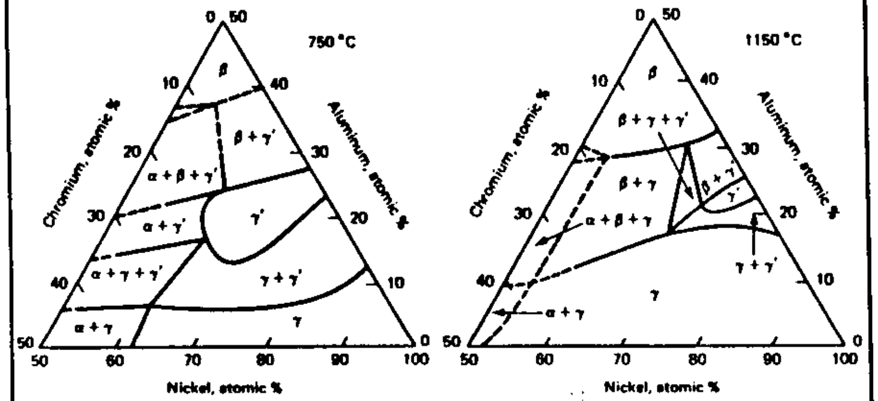

Fig. 5-15. Isothermal sections at 750 and 1150 °C from the Ni-Cr-Al phase diagram. (Adapted from A. Taylor and R. W. Floyd, J. Inst. Metals, Vol 81, p 455 and 460, 1952-53)

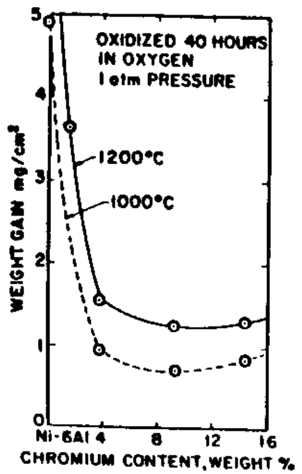

Fig. 5-19. Effect of Cr content on the oxidation of Ni-Cr-Al alloys of fixed Al content (6%). (From I. A. Kvernes and P. Kofstad, Met. Trans., Vol 3, p 1518, 1972)

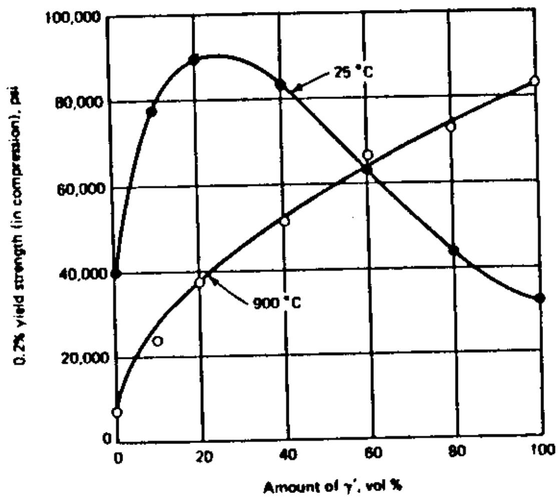

Fig. 5-17. Effect of the amount of γ' in Ni-Cr-Al alloys of fixed Ni content (75%) on the yield strength (in compression tests) measured at 25 °C and at 900 °C. All alloys were solution heat treated at 1150 °C for 2 h, air cooled at 25 °C, then aged for 16 h at 900 °C to develop the equilibrium phases. (Adapted from same source as Fig. 5-16, bottom diagram)

COMPLEX NICKEL-BASE SUPERALLOYS:

PHYSICAL METALLURGY AND ALLOY DESIGN

PHYSICAL METALLURGY AND ALLOY DESIGN OF Ni-BASE SUPERALLOYS

- THE MICROSTRUCTURAL FEATURE THAT IS COMMON TO ALL Ni-BASE SUPERALLOYS IS THE DISPERSION OF γ' IN A γ MATRIX ALONG WITH VARIOUS CARBIDES.
- METALLURGICAL FACTORS AFFECTING THE CREEP AND TENSILE PROPERTIES OF Ni BASE SUPERALLOYS
  - SOLID SOLUTION HARDENING OF γ PHASE
  - SOLID SOLUTION HARDENING OF γ' PHASE
  - DISPERSION OF γ': PARTICLE SIZE AND SHAPE, PARTICLE SPACING, INTERFACIAL AREA PER UNIT VOL.
  - VOLUME FRACTION OF γ'
  - STABILITY OF γ' UNDER STRESS AND TEMPERATURE
  - LATTICE MISMATCH BETWEEN γ AND γ'
  - ANTIPHASE BOUNDARY ENERGY
  - PRECIPITATION OF CARBIDE-TYPE PHASES
- OXIDATION AND HOT CORROSION RESISTANCE

Table 5-3. List of Important Factors To Consider in the Design of Ni-Base Superalloys

Phase relation/property	Effect	Reference
1. Solid solution strengthening of γ	W, Mo, Ti, Al, Cr strengthen; Fe, Co, Cu strengthen slightly	Fig. 5-5, Table 5-1
2. Solid solution strengthening of γ'	Mo, W, Si, Ti, Cr strengthen; V, Co weaken; Mn, Fe, Cu strengthen slightly	Fig. 5-27
3. Amount of γ'	Cr, Ti, Al, Nb, Mo, Co, Ta, V, Fe increase	Fig. 5-31 to 5-36
4. Antiphase boundary energy	Ti, Co, Mo, Fe increase; Al, Cr decrease	Table 5-4
5. γ-γ' lattice mismatch	Ta, Nb, C, Ti increase; Cr, Mo, W, Cu, Mn, Si, V decrease; Al, Fe, Co negligible effect	Fig. 5-39 to 5-44
6. Coarsening rate of γ'	Mo, Cr, Nb decrease; Ti, Al increase; Co, Fe slight effect; Zr, B no effect	Fig. 5-47
7. Oxidation and hot corrosion resistance	Cr improves; other elements variable	Fig. 5-47 and 5-48

Note. Numbers in first column relate to text discussion. Information after R. F. Decker, in Steel Strengthening Mechanisms, Climax Molybdenum Company, Greenwich, Conn., 1969.

SOLID-SOLUTION STRENGTHENING OF γ PHASE

- INCREASE THE MELTING POINT
- DECREASE IN DIFFUSION RATE
- ATOMIC SIZE DIFFERENCE

Table 5-1. Approximate Atom Diameter Size Difference and Approximate Solubility in Ni of Several Solutes

Solute	Approximate atom diameter size difference, % $(d_{so} - d_{Ni})/d_{Ni}$	Approximate solubility in Ni at 1000 °C, wt %	Solute	Approximate atom diameter size difference, % $(d_{so} - d_{Ni})/d_{Ni}$	Approximate solubility in Ni at 1000 °C, wt %
C	+43	0.2	Fe	+0.3	100
Al*	−15	7	Co	−0.2	100
Si	+6	8	Cu	−3	100
Ti*	−17	10	Nb*	−15	6
V	−6	20	Mo*	−9	34
Cr	−0.3	40	Ta*	−15	14
Mn*	+10	20 (at 500 °C)	W*	−10	38

Note. Solutes marked with an asterisk (*) show the best combination of large size difference and high solubility and should be the most potent solid solution strengtheners.

$\frac{D\sigma}{DC}$ ~ SIZE DIFFERENCE

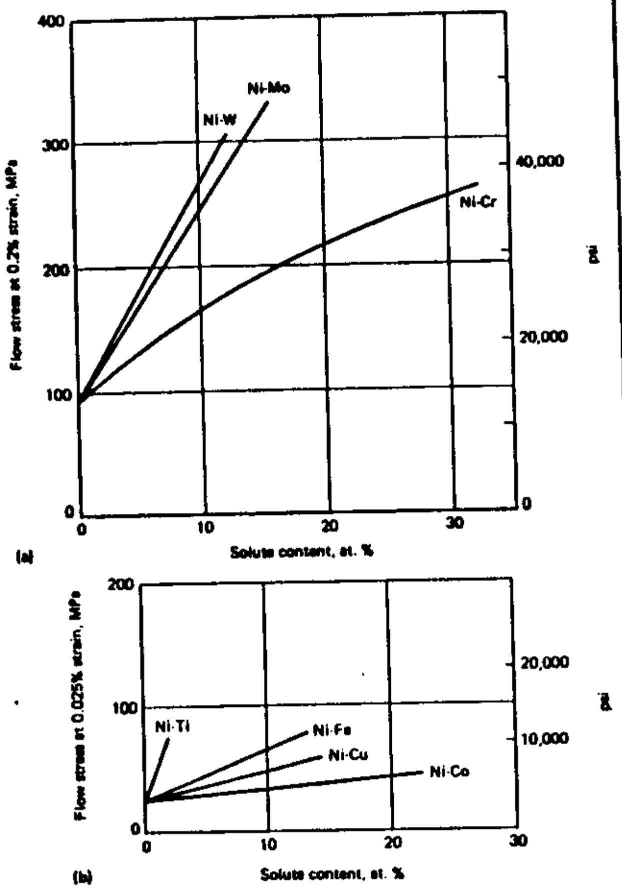

Fig. 5-5. Effect of solute content of Ni on yield strength (flow stress) at 25 °C. The alloys were all solid solution, single-phase. (a) adapted from R. M. N. Pelloux and N. J. Grant, Trans. Met. Soc. AIME, Vol 218, p 232, 1960; (b) adapted from E. R. Parker, in Relation of Properties to Microstructure, American Society for Metals, Metals Park, Ohio, 1954.

SOLID-SOLUTION STRENGTHENING OF γ'

- SOLUBILITY LIMIT
- LATTICE STRAIN: DA/DC

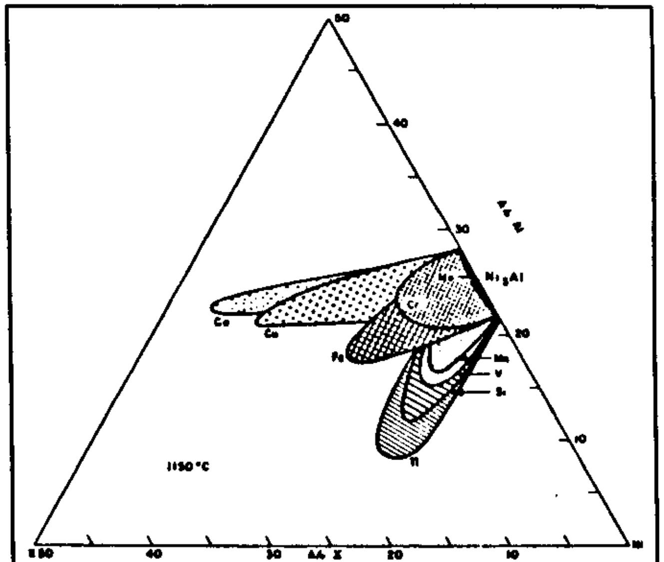

Fig. 5-28. Ternary phase diagrams of Ni-Al-X showing the effect of the element X on the size of the γ' field at 1150 °C. (From same source, p 810, as Fig. 5-24)

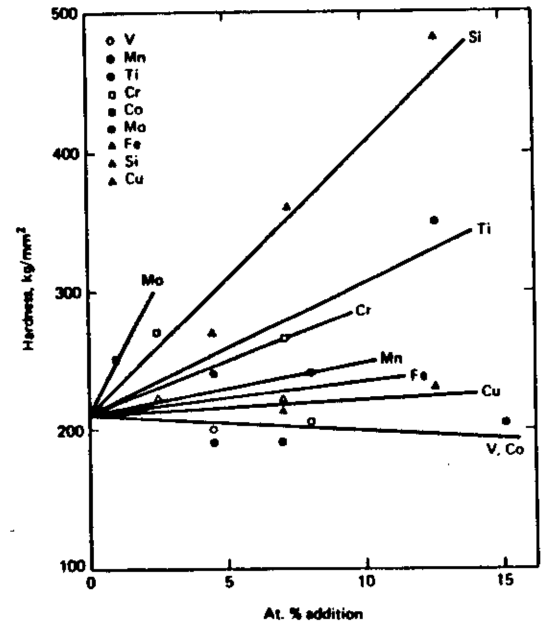

Fig. 5-27. Effect of alloying elements dissolved in γ' on the hardness at 25 °C. (From same source as Fig. 5-24)

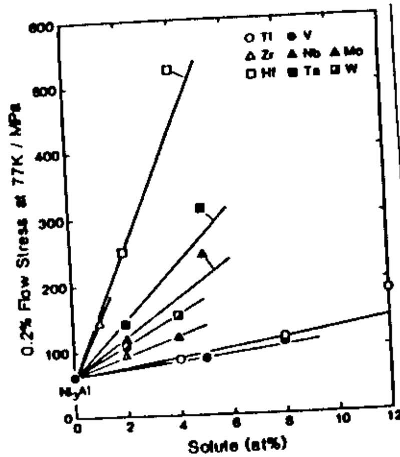

Fig. 9 Relation between 0.2% flow stress measured at 77 K and the solute concentration in ternary Ni_3Al with addition of transition metal elements.

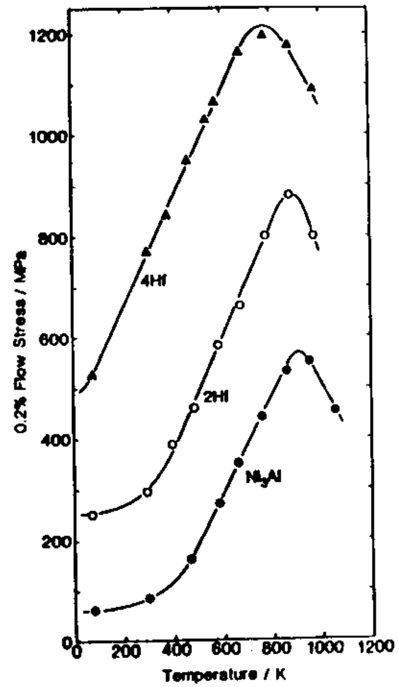

Fig. 3 Temperature dependence of 0.2% flow stress in Ni_3Al with addition of Hf.

ANTIPHASE BOUNDARY (APB) ENERGY

- THE DEVELOPMENT OF APB WHEN A DISLOCATION ENTERED AN ORDERED PARTICLE
- FOR BEST STRENGTHENING, IT IS DESIRED TO HAVE HIGH APB ENERGY
- APB ENERGY OF γ' IN DIFFERENT ALLOYS

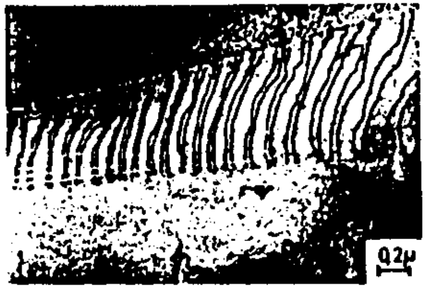

Aged 1 h at 750 °C, deformed 2%.
The fine γ' is not resolved here.

Aged 540 h at 750 °C, deformed 3%.

Fig. 5-38. Transmission electron micrographs illustrating the interaction of ordered precipitates and dislocations as depicted in Fig. 5-37. In (a) the dislocations are moving as pairs through a very dense, fine, ordered γ' precipitate dispersion. (b) illustrates the cutting of the particles by dislocations. The alloy contained 84Ni-16Cr-7.5Al (at.%). (Adapted from H. Gleiter and E. Hornbogen, Acta Met., Vol 13, p 577, 1965)

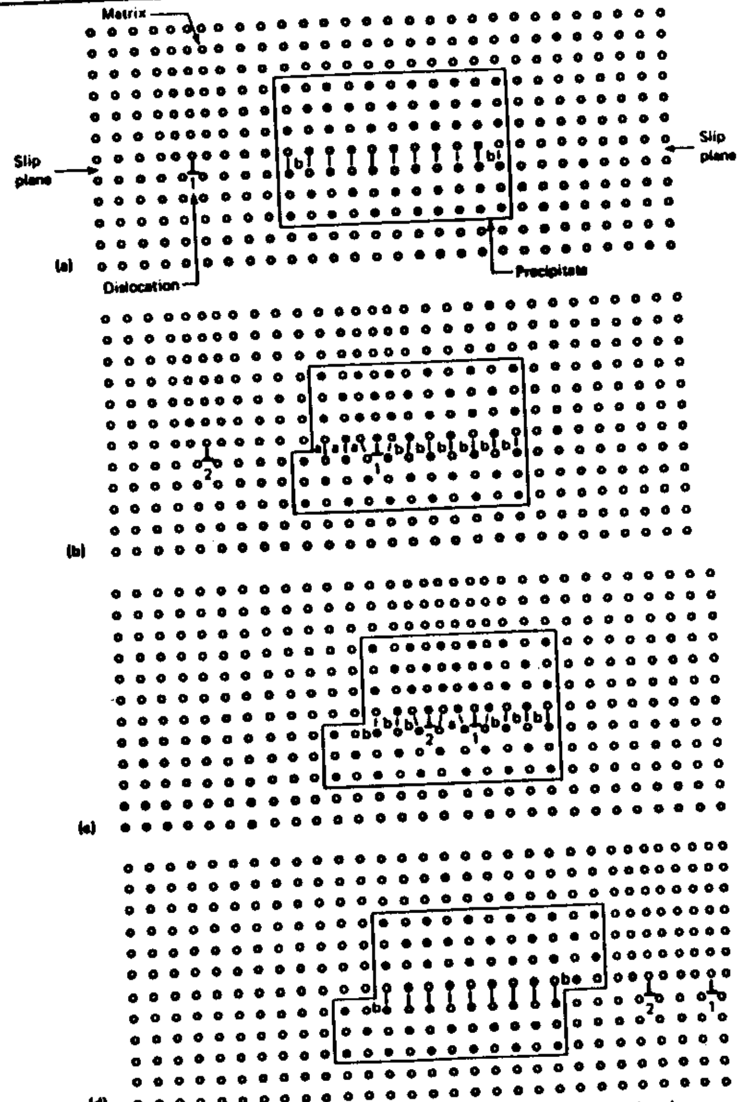

Fig. 5-37. Schematic illustration of the development of repulsive bonding (marked a) if a dislocation enters an ordered precipitate particle, and the minimization of the number of such bonds if the dislocations move in pairs through the precipitate.

Table 5-4. Approximate Antiphase Boundary Energy of γ' in Different Alloys

Alloy composition	APB energy, erg/cm²
Ni-12.7 to 14.0Al (at. %)	153
Ni-18.5Cr-7.5Al (at. %)	104
Ni-8.8Cr-6.2Al (at. %)	90
Fe-Cr-Ni-Al-Ti	
Ti/Al = 1	240
Ti/Al = 8	300
Ni-19Cr-14Co-7Mo-2Ti-2.3Al (at. %)	170-220
Ni-33Fe-16.7Cr-3.2Mo-1.6Al-1.1Ti (wt %)	270

Adapted from N. S. Stoloff, in The Superalloys, ed. C. T. Sims and W. C. Hagel, Wiley, New York, 1972.

- Ti, Co, and Fe increase APB energy
  Al and Cr decrease APB energy

γ − γ' LATTICE MISMATCH

- THE γ − γ' LATTICE MISMATCH IS AFFECTED BY BOTH PARTITIONING AND ATOM SIZE OF ALLOYING ELEMENTS

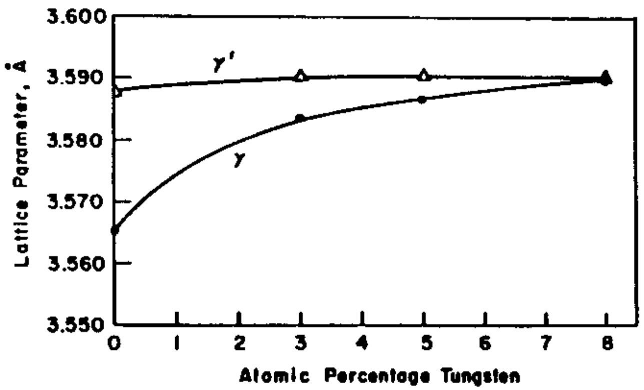

Figure 16.
Influence of W additions upon the lattice parameters of both the γ and γ' phases in a Ni-20 at.% Cr-5 at.% Al-5 at.% Ti alloy(ref.33).

- GENERALLY, HIGH MISMATCH MEANS HIGH TENSILE STRENGTH, BUT AT HIGH TEMPERATURES THE γ' PARTICLES TEND TO COALESCE MORE RAPIDLY THE HIGHER THE MISMATCH, AND THUS FOR CREEP APPLICATIONS LOW MISMATCH IS DESIRED

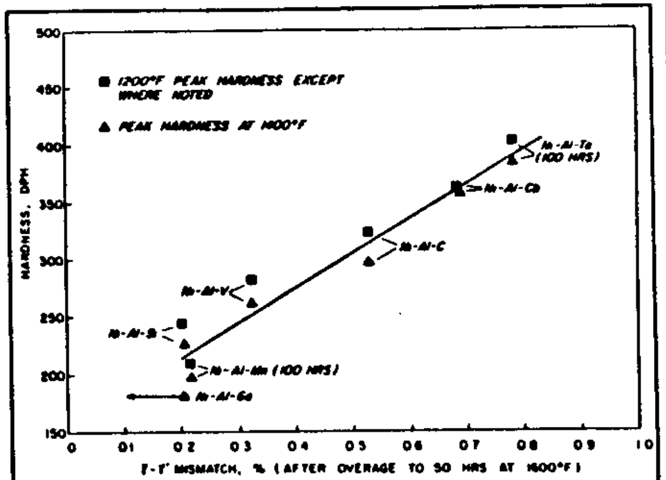

Fig. 5-39. Correlation of peak aged hardness with γ-γ' lattice mismatch for several Ni-Al-X ternary alloys. The hardness was measured at 25 °C. (From R.F. Decker and J.R. Mihalisin, Trans. ASM, Vol 62, p 485, 1969)

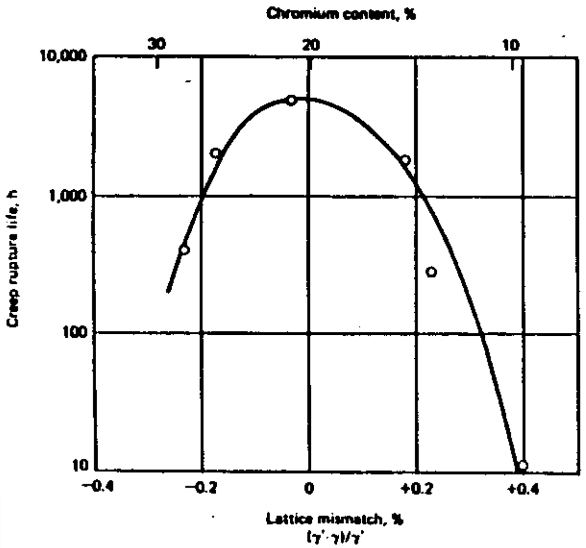

Fig. 5-18. Effect of lattice mismatch between γ and γ' on the creep rupture life at 21,200 psi and 700 °C for Ni-Cr-Al alloys. The Al content was approximately constant at 7 at.%. (Adapted from I.L. Mirkin and O.D. Kancheev, Metal Sci. and Heat Treat., No. 1, p 10, 1967)

γ – γ' LATTICE MISMATCH

- THE LATTICE MISMATCH AFFECTS THE MORPHOLOGY OF THE γ' PRECIPITATES

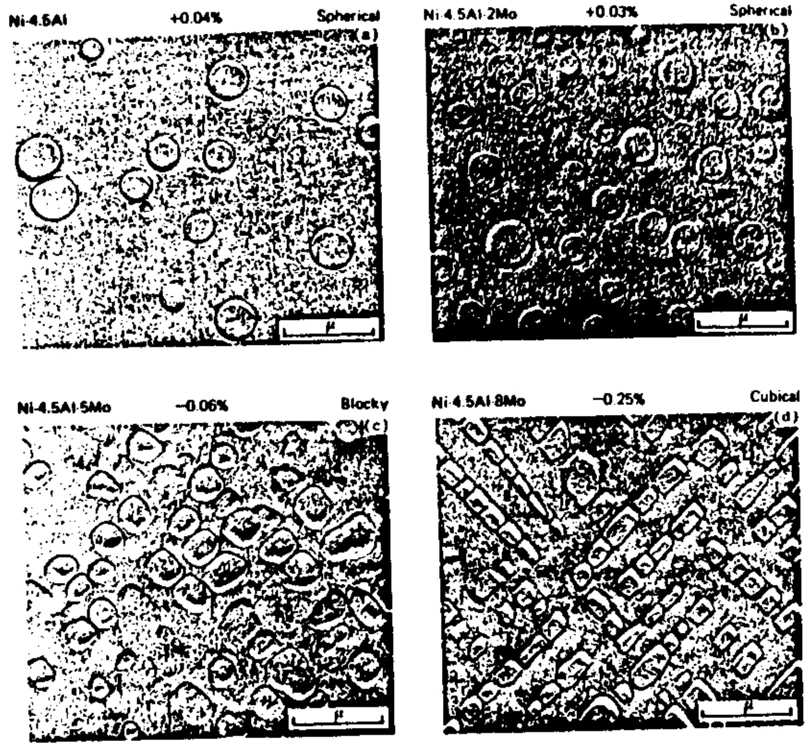

Fig. 5-45. Effect of Mo content on the γ' morphology in Ni-Al-Mo alloys. The alloys were aged for 112 h at 925 °C. The γ'-γ lattice mismatch values are shown, as well as the description of the γ' morphology. All compositions, wt %. (Adapted from V. Biss and D. L. Sponseller, Met. Trans., Vol 4, p 1956, 1973)

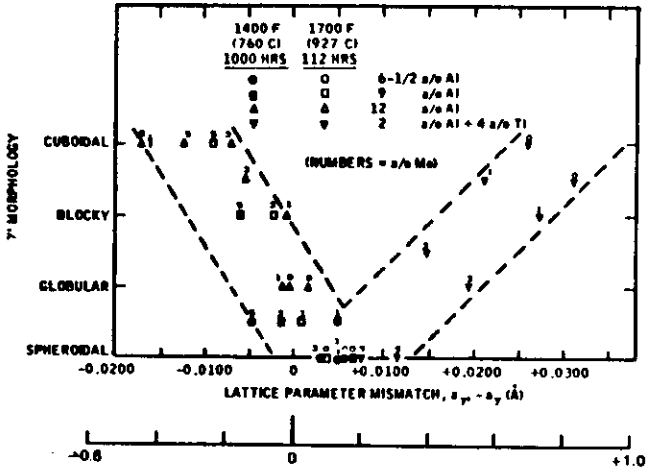

Fig. 5-46. Influence of lattice mismatch between γ and γ' and the γ' precipitate morphology for Ni-Al-Ti-Mo alloys. All compositions, at.%. (Adapted from same source as Fig. 5-32)

COARSENING RATE OF γ'

- PARTICLE SIZE VARIES WITH THE AGING TIME TO THE ONE-THIRD POWER

$$D = K\tau^{1/3}$$

$$K = \left[\frac{64 r D C_0 V_M^2}{9\ RT}\right]^{1/3}$$

- THE COARSENING RATE INCREASES WITH INCREASING THE LATTICE MISMATCH

- IN GENERAL, AL AND TI INCREASE THE COARSENING RATE, AND MO, CR AND NB DECREASE IT

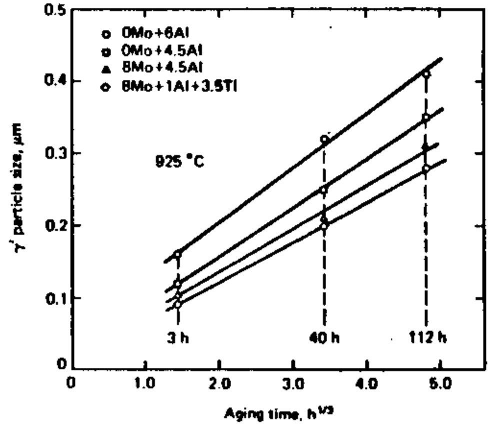

Fig. 5-47. γ' particle size of Ni-Mo-Al and Ni-Mo-Al-Ti alloys as a function of aging time to the 1/3 power. All compositions, wt %. (Adapted from same source as Fig. 5-45)

- THE VOLUME FRACTION OF γ´ PRECIPITATES DEPENDS MAINLY UPON THE AT. % OF THE γ´ FORMING ELEMENTS AL, TI, NB, TA, V, HF, AND ZR PRESENT

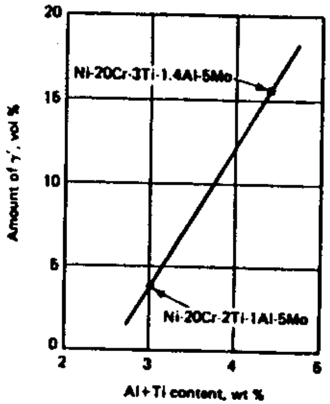

Fig. 5-35. Effect of Al and Ti content on the amount of γ´ in Ni-Cr-Al-Ti-Mo alloys. The alloys were aged for 50 h at 900 °C after solution treatment at 1120 °C. (Adapted from same source as Fig. 5-33)

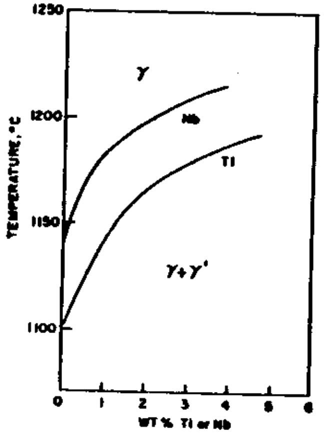

Figure 5.
Influence of replacing Al by Ti or Nb upon the γ' solvus temperature.

- THE REPLACEMENT OF AL BY EITHER TI OR NB RESULTS IN A CONSIDERABLE INCREASE IN THE γ´ SOLVUS TEMPERATURE

- THE ADDITION OF Co GENERALLY RAISES THE SOLUBILITY CURVE IN TEMPERATURE, RESULTING IN INCREASE IN THE AMOUNT OF γ´ AT A GIVEN TEMPERATURE

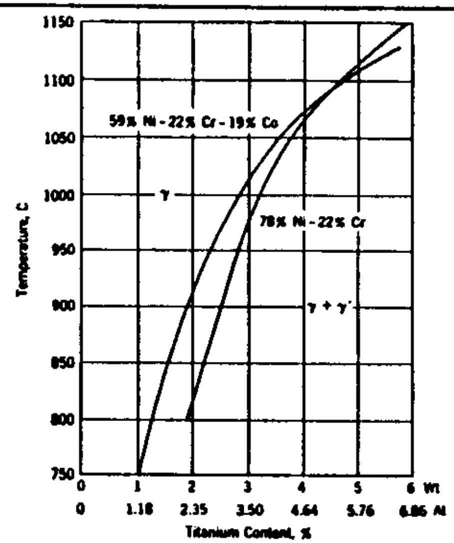

Fig. 5-36. Isopleth sections of the ternary Ni-Cr-Ti and the quaternary Ni-Cr-Co-Ti phase diagrams, at 22% Cr. (From J. Heslop, Cobalt, Vol 24, p 128, 1964)

STRENGTHENING EFFECTS OF γ′ PRECIPITATION

- HIGH-TENSILE STRENGTH OF γ′ – ANOMALOUS TEMPERATURE DEPENDENCE OF FLOW STRESSES OF γ′
- HIGH γ – γ′ MISMATCH MEANS HIGH TENSILE STRENGTH
- RESISTANCE TO DISLOCATION CUTTING THROUGH – HIGH APB ENERGY
- THE IMPEDENCE PROVIDED BY THE γ/γ′ INTERFACE FURNISHED A BASIS FOR STORING DISLOCATIONS IN THE FORM OF A FINE CELLULAR NETWORK. THE GREATER THE INTERFACIAL AREA PER UNIT VOLUME, THE HIGHER THE PLASTIC RESISTANCE AT LOW STRAIN RATES
- THE STRENGTH AT ELEVATED TEMPERATURES INCREASES WITH THE VOLUME FRACTION OF γ′

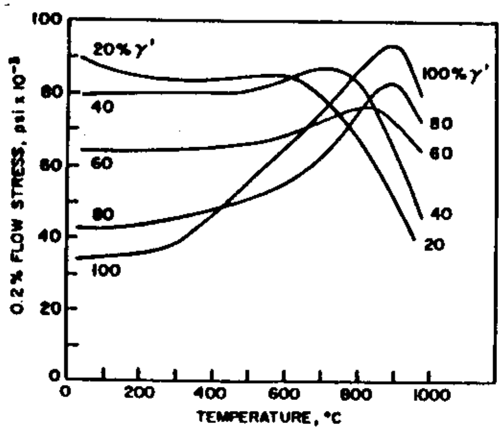

Figure 7.
The temperature dependence of the 0.2% flow stress for Ni-Cr-Al alloys containing different volume fractions of γ' (ref. 24).

THE CREEP IN γ + γ′ ALLOYS – CONDITIONS FOR ACHIEVING MAXIMUM CREEP RESISTANCE

- VOLUME FRACTION OF γ′ PHASE TO BE AROUND 60%
- INTERPARTICLE SPACING TO BE OF THE ORDER OF 500 Å
- THE PARTICLE SHOULD HAVE A STRENGTH GREATER THAN THAT OF MATRIX TO MINIMIZE CUTTING THROUGH
- SMALL LATTICE MISMATCH BETWEEN PARTICLE AND MATRIX TO PROMOTE STABILITY
- GOOD THERMAL STABILITY OF THE γ′ STRUCTURE
- MAXIMIZING SOLID SOLUTION HARDENING THE γ MATRIX

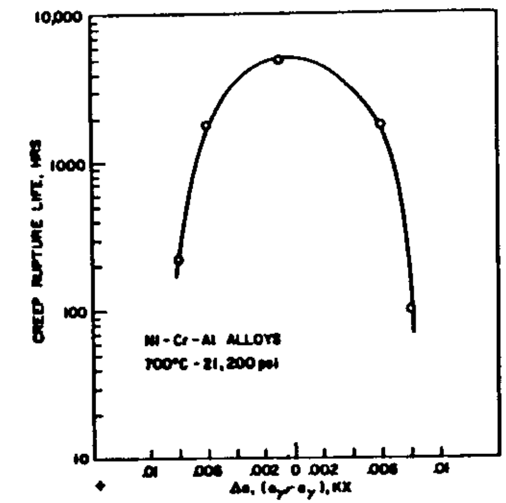

Figure 14.
Influence of lattice mismatch, Δa, upon creep rupture life (ref. 31).

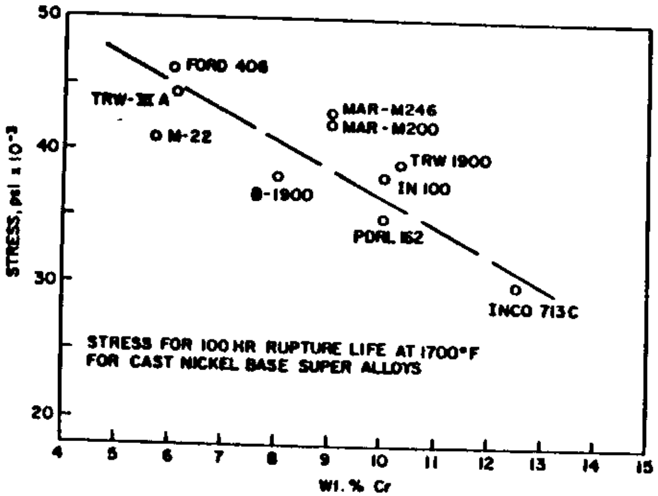

Figure 17.
Creep rupture strength at 1700°F as a function of chromium content for cast nickel base superalloys.

SCHEMATIC ILLUSTRATION OF THE FORMATION OF THE AS-CAST STRUCTURE OF IN-100

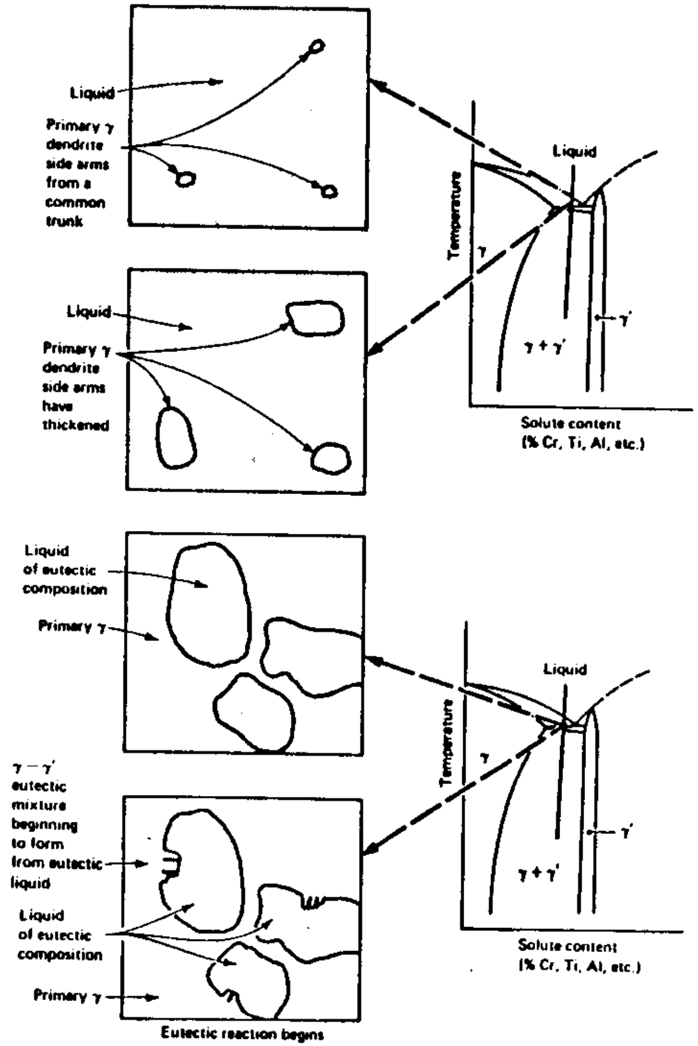

Fig. 5-78. Schematic illustration of the formation of the as-cast structure of IN-100. See text for explanation.

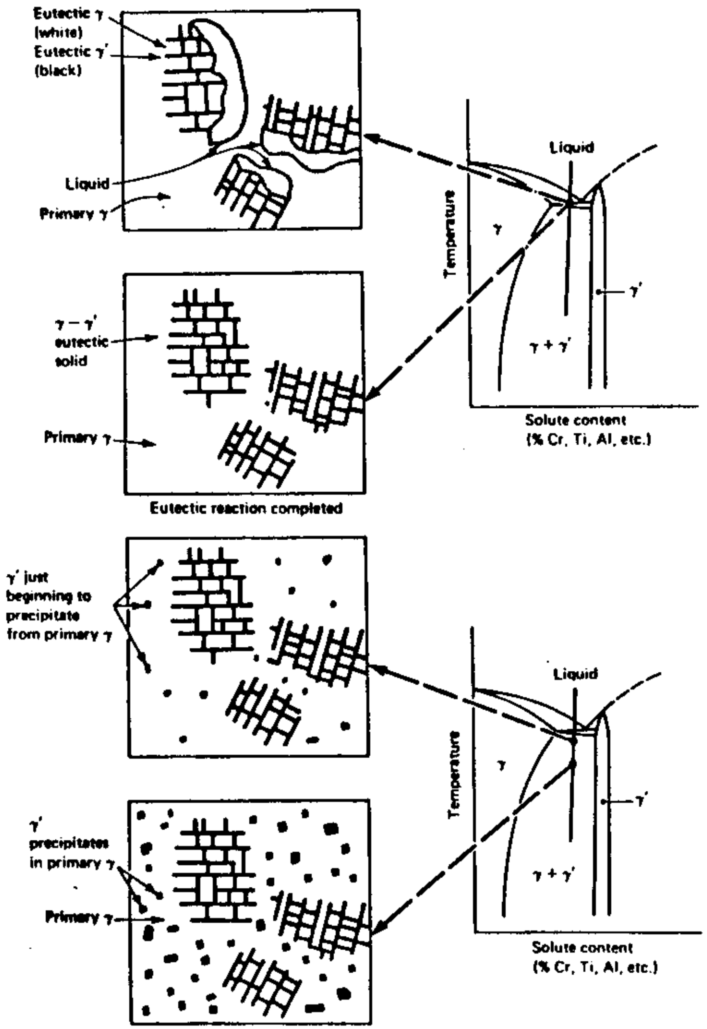

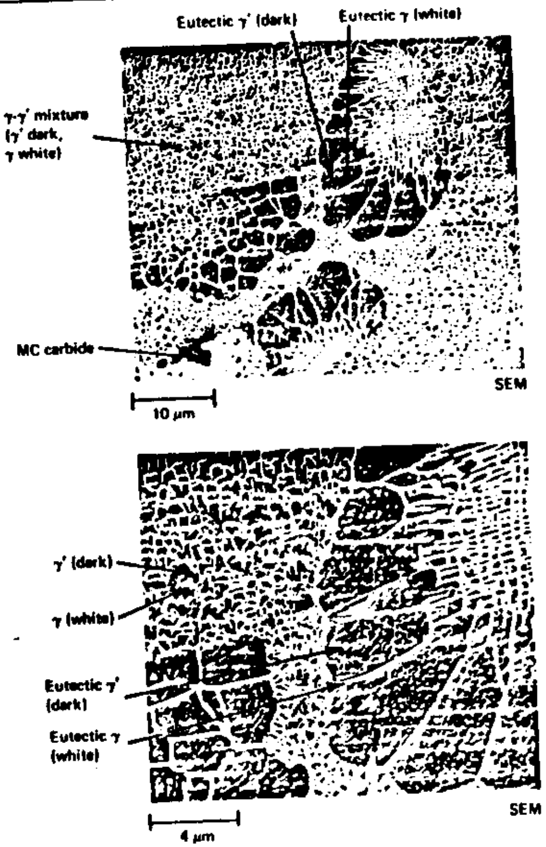

Fig. 5-79. Higher-magnification views showing distinctly the γ and γ' structure of the as-cast IN-100 alloy.

COMPLEX MICROSTRUCTURES OF CAST NICKEL-BASE SUPERALLOYS

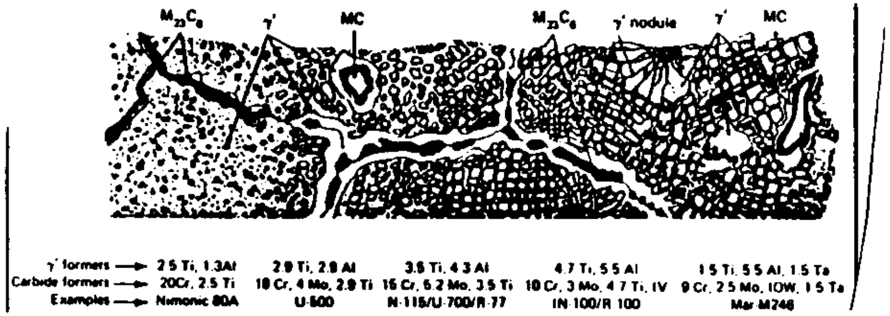

COMMON DESIRABLE MICROSTRUCTURE

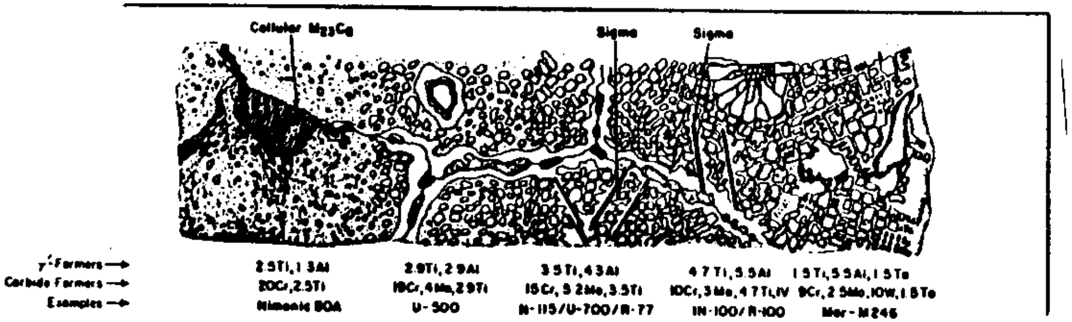

COMMON UNDESIRABLE MICROSTRUCTURE

FUNCTION OF CARBON AND CARBIDE IN Ni-BASE SUPERALLOYS

- GB SCAVENGER
  - IT APPEARS THAT C (>0.02%) MUST BE PRESENT DURING THE SOLIDIFICATION TO MAKE CERTAIN THAT HARMFUL TRACE ELEMENTS SUCH AS O_2 AND S DO NOT COLLECT IN THE GB AND PRODUCE BRITTLE FILMS
  - B, Zr AND THE RARE EARTH ELEMENTS PROBABLY FUNCTION IN A SIMILAR WAY
- CARBIDE FORMATION
  - ONCE THE ALLOY HAS SOLIDIFIED IT IS DESIRABLE TO HAVE THE C COMBINED IN THE FORM OF A VERY STABLE CARBIDE
  - HOWEVER, FOR MANY OF THE CAST NICKEL-BASE ALLOYS, THE MC (TaC, TiC, NbC) CARBIDES FORMED DURING SOLIDIFICATION PROCESS DECOMPOSE IN SERVICE AT 800 TO 930°C TO GIVE $M_{23}C_6$ (Cr RICH MAY CONTAIN SOME Mo AND W) AND M_6C (Mo AND W RICH) CARBIDES. A COMMON REACTION IS

$$MC + \gamma \rightarrow M_{23}C_6 + \gamma'$$

$$(Ti,Mo)C + (Ni,Cr,Al,Ti) \rightarrow (Cr,Mo)_{23}C_6 + Ni_3(Al,Ti)$$

CONTROL OF TCP PHASES

- AN UNDESIRABLE FEATURE OF THE MOST HIGHLY ALLOYED SUPERALLOYS IS THEIR TENDENCY TO DEVELOP UNWANTED TCP PHASES SUCH AS SIGMA AND MU.
- THE FORMATION OF TCP PHASES THAT TAKE Mo AND W OUT OF THE MATRIX WILL SIMILARLY UNBALANCE THE ALLOY AND DEGREDATE THE CREEP PROPERTIES. LOW TEMPERATURE DUCTILITY ALSO IS AFFECTED ADVERSELY.
- SIGMA AND OTHER TCP PHASES ARE ELECTRON COMPOUNDS WHOSE PRECIPITATION FROM SOLUTION CAN BE PREDICTED BY KNOWLEDGE OF THE AVERAGE ELECTRON – VACANCY NUMBER OF THE ALLOY MATRIX.
- THE "PHACOMP" SYSTEM – THE γ SOLUTION BECOMES UNSTABLE AND STARTS TO PRECIPITATE σ PHASE WHEN A CRITICAL ELECTRON VACANCY NUMBER (2.5) IS EXCEEDED. TO AVOID σ PRECIPITATION DURING ALLOY PROCESSING OR IN SERVICE, THE TOTAL CONCENTRATION OF ELEMENTS WITH HIGH ELECTRON VACANCY NUMBER (Cr, Mo, W, Mn) MUST BE LIMITED TO A LOW LEVEL.
- COMPUTER PROGRAMS DERIVED FROM THE PRINCIPLES OF ELECTRON-VACANCY NUMBERS AND PHASE STABILITY ARE NOW USED IN SUPERALLOY ENGINEERING SPECIFICATIONS.

Table 5-7. Possible Electron Hole Numbers ($\bar{N}_v$) for Several Elements

Group →	VIA	VIIA	VIIIA		
First long period	Cr (4.66)	Mn (3.66)	Fe 2.22	Co 1.71	Ni 0.61
Second long period	Mo (4.66)	Tc (3.66)	Ru (2.66)	Rh (1.66)	Pd (0.66)
Third long period	W (4.66)	Re (3.66)	Os (2.66)	Ir (1.66)	Pt (0.66)

From C. T. Sims, in *The Superalloys*, ed. C. T. Sims and W. C. Hagel, Wiley, New York, 1972.

INNOVATIVE MATERIALS SYNTHESIS

1. DIRECTIONAL SOLIDIFICATION
2. RAPID SOLIDIFICATION
3. MECHANICAL ALLOYING
4. DIRECTIONAL SOLIDIFIED EUTECTICS

DIRECTIONAL SOLIDIFICATION PROCESSING

- GRAIN BOUNDARY SLIDING AND VOID FORMATION OCCUR ALONG BOUNDARIES NORMAL TO THE STRESS AXIS, LEADING TO HIGH CREEP RATES AND PREMATURE FRACTURE IN EQUIAXED POLYCRYSTALLINE MATERIALS

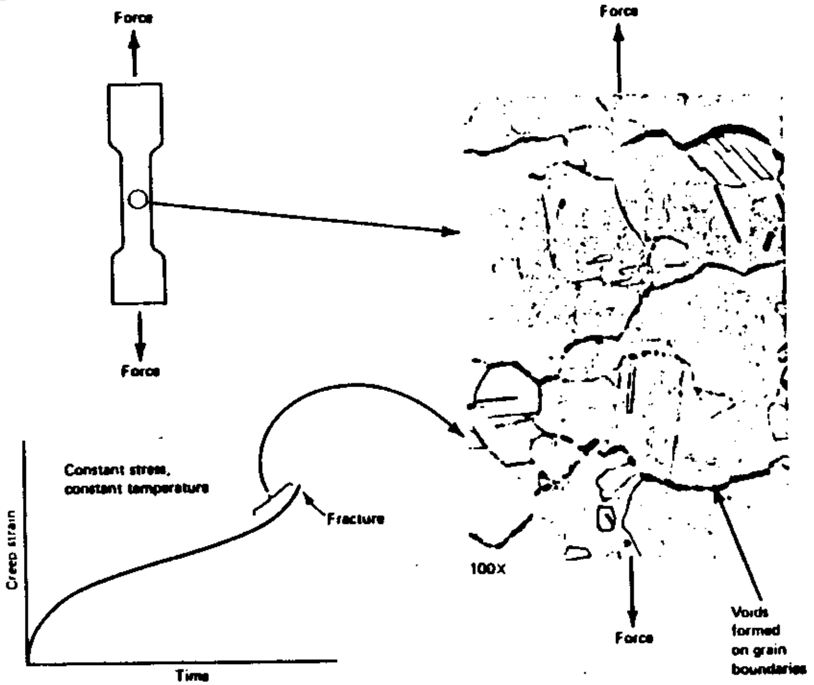

Fig. 5-61. Illustration of void formation on grain boundaries which are mainly normal to the stress axis. The microstructure was taken from a sample of copper creep tested at 385 °C under a stress of 2500 psi. The schematic sketches show the relation of the microstructure to the creep test specimen and to the final stage of creep in which the voids form. (Microstructure from F.L. VerSnyder, in High Temperature Materials, ed. R.F. Hehemann and G.M. Ault, Wiley, New York, 1959)

COMPARISON OF CREEP CURVES

OF MAR-M200 IN THE POLYCRYSTALLINE EQUIAXED (A), [001] COLUMNAR (B), AND [001] SINGLE-CRYSTAL (C) STRUCTURES

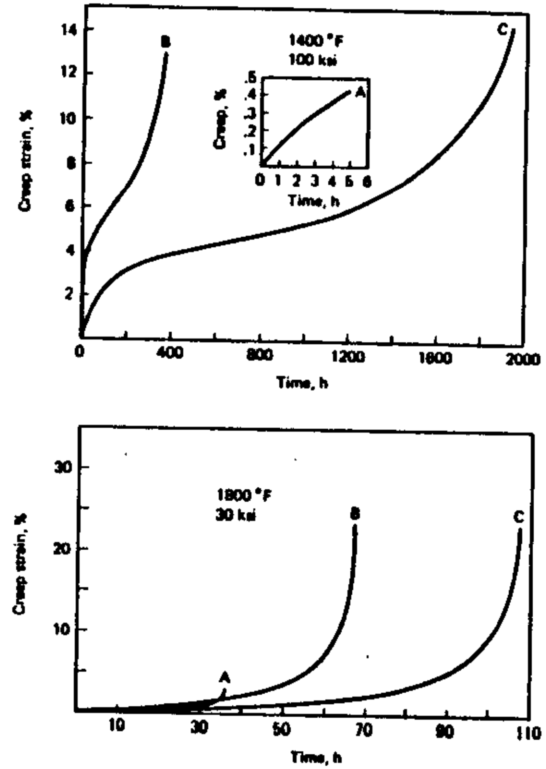

Fig. 5-68. Comparative creep curves of Mar-M200 in the polycrystalline equiaxed (A), [001] columnar (B) and [001] single-crystal (C) structures. (From same source as Fig. 5-64)

SCHEMATIC ILLUSTRATION OF THE FORMATION OF COLUMNAR GRAINS EACH HAVING A [1̄00] ORIENTATION

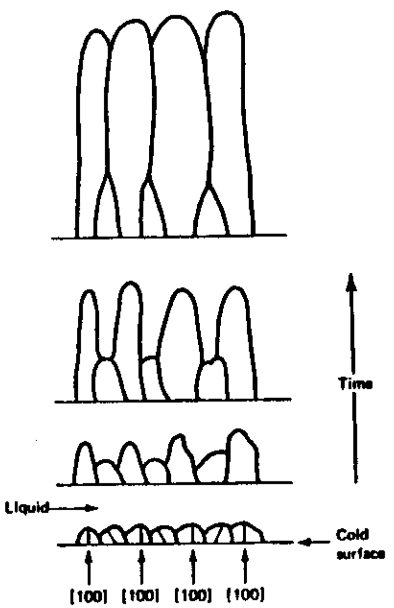

Fig. 5-70. Schematic illustration of the formation of columnar grains each having a [100] orientation. Each columnar grain is oriented randomly about the vertical axis. The [100] axis in each nucleated grain is shown by the line. Arrows indicate those with the [100] vertical.

ILLUSTRATION OF A METHOD OF INVESTMENT SHELL MOLD CASTING OF DIRECTIONALLY SOLIDIFIED GAS-TURBINE BLADES

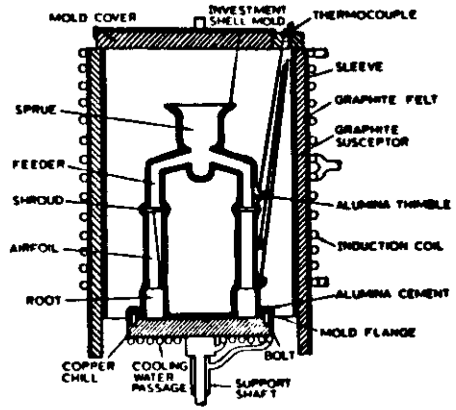

Induction-heated, investment shell mold assembly for casting directionally solidified gas-turbine blades

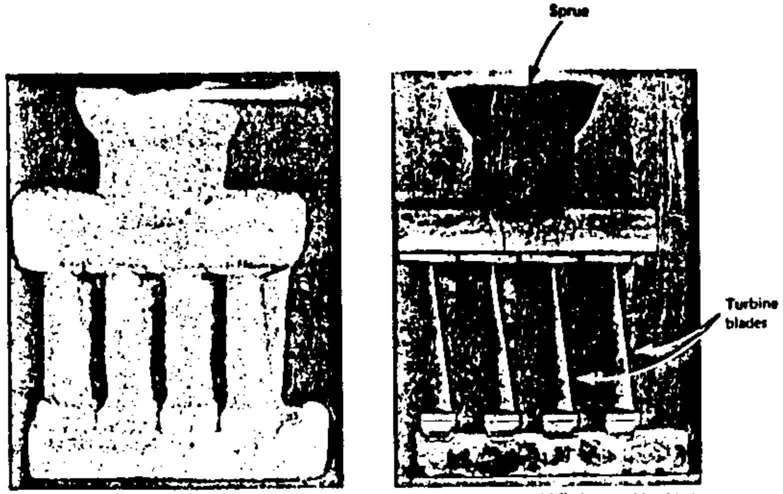

Four-blade silica investment shell mold

Four directionally solidified gas-turbine blades

Fig. 5-71. Illustration of a method of investment shell mold casting of directionally solidified gas-turbine blades. (Adapted from F.L. Ver-Snyder and M.E. Shank, Mater. Sci. Eng., Vol 6, p 213, 1970)

DIRECTIONALLY SOLIDIFIED GAS TURBINE VANE CONSISTING OF COLUMNAR GRAINS

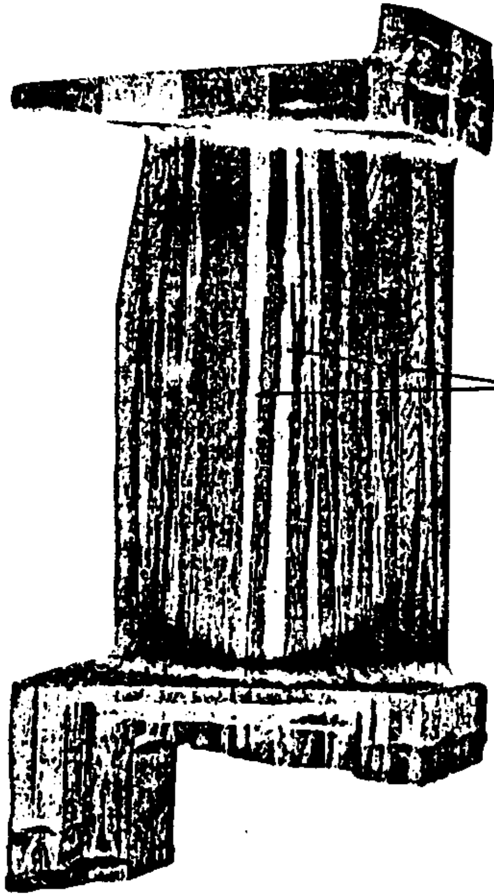

Fig. 5-72. Directionally solidified gas-turbine vane consisting of columnar grains, revealed by macroetching. (Adapted from same source as Fig. 5-67)

SOLIDIFICATION SEQUENCE AND MOLD DESIGN WHICH LEAD TO SINGLE CRYSTAL GROWING IN THE REGION OF THE CONSTRICTOR

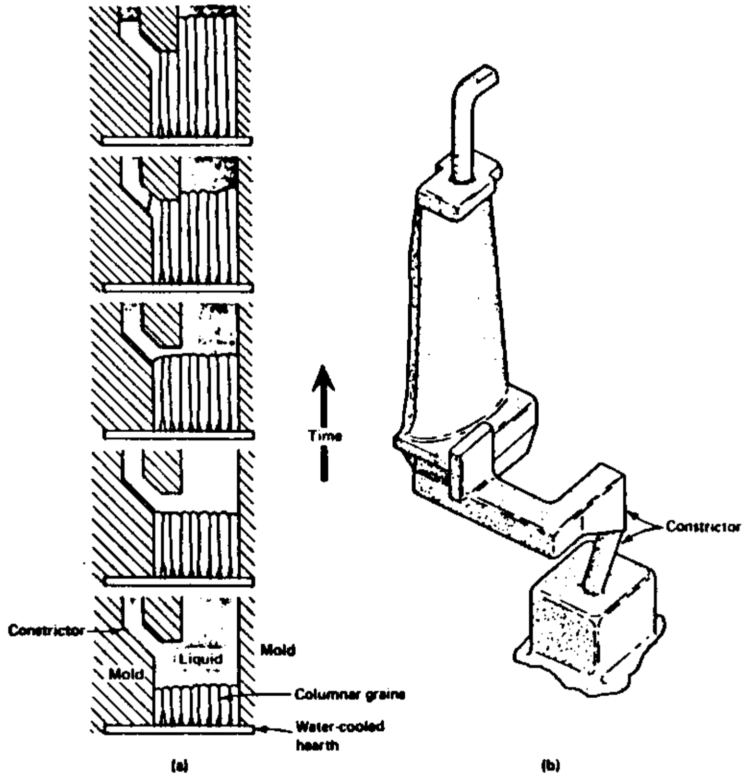

Fig. 5-73. (a) Schematic illustration of the solidification sequence which leads to a single crystal growing in the region of the constrictor. The mold cavity (or the object being cast (e.g., a turbine blade) would be connected to the constrictor. (b) Constriction mold producing cast, single-crystal gas-turbine blades. (Adapted from same source as Fig. 5-71)

ILLUSTRATION OF USE OF MULTIPLE CONSTRICTION INVESTMENT CASTING TECHNIQUE TO CAST SINGLE-CRYSTAL GAS-TURBINE BLADES

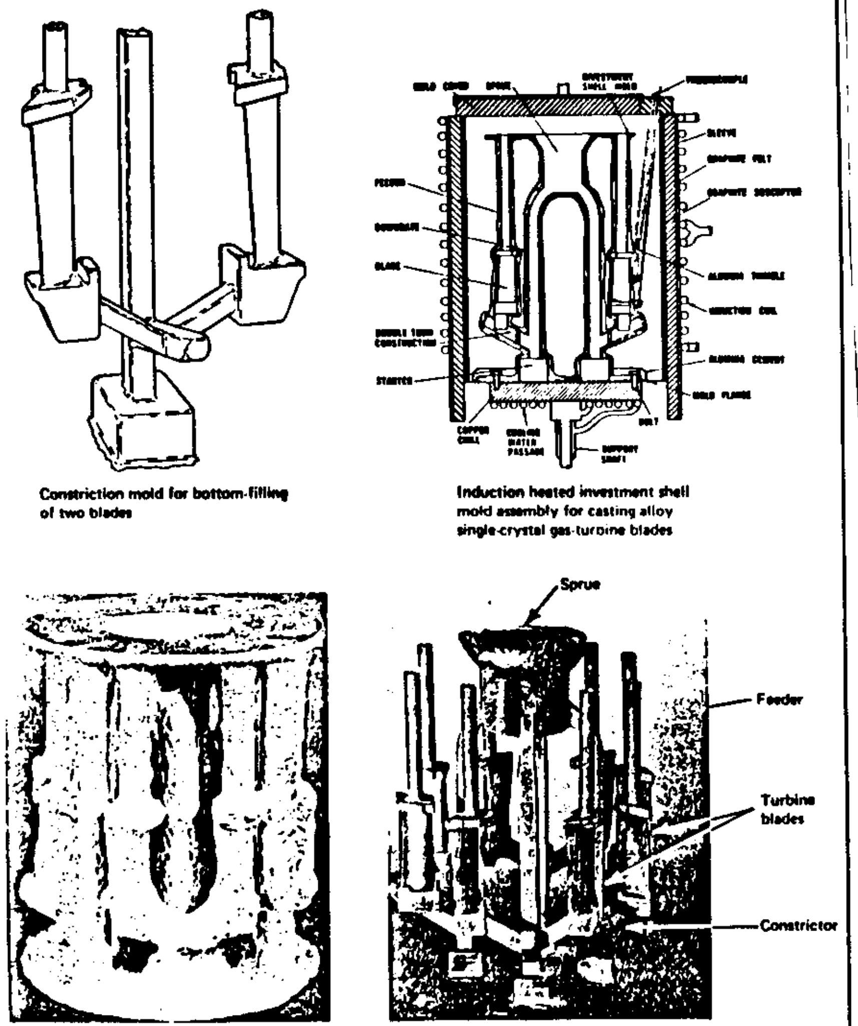

Constriction mold for bottom-filling of two blades

Induction heated investment shell mold assembly for casting alloy single-crystal gas-turbine blades

Multiple constriction, competitive growth investment shell mold

Multiple constriction, competitive growth investment casting of eight alloy single-crystal gas-turbine blades

Fig. 5-74. Illustration of use of multiple constriction investment casting technique to cast single-crystal gas-turbine blades. (Adapted from same source as Fig. 5-71)

MECHANICAL ALLOYING PROCESSING AND APPLICATION TO ODS ALLOYS

- ODS ALLOYS ATTRACT GREAT ATTENTION AS ADVANCED HT MATERIALS BECAUSE THEY CAN RETAIN USEFUL STRENGTH UP TO A RELATIVELY HIGH FRACTION OF THEIR T_m.

- CONVENTIONAL POWDER METALLURGY TECHNIQUES, FOR INSTANCE, EITHER DO NOT PRODUCE AN ADEQUATE DISPERSION, OR DO NOT PERMIT THE USE OF REACTIVE ALLOYING ELEMENTS SUCH AS Al, Ti, AND Cr. MA PROCESSING HAS BEEN INTRODUCED TO SOLVE THESE DIFFICULTIES.

- MA IS A HIGH ENERGY, DRY MILLING PROCESS IN WHICH A MIXTURE OF METAL AND/OR NONMETAL POWDERS ARE SUBJECTED TO CONSTANT FRACTURING AND REWELDING IN AN ENERGETIC GRINDING BALL CHARGE. DURING EACH COLLISION OF THE GRINDING BALLS, MANY POWDER PARTICLES MAY BE SIMULTANEOUSLY TRAPPED, WELDED TOGETHER, PLASTICALLY DEFORMED, AND FRACTURED (FIG. 29).

  THE REPETITION OF THESE "MA EVENTS" OVER A SUFFICIENT TIME PERIOD RESULT IN A HOMOGENEOUS SUPERALLOY POWDER IN WHICH THE CONSTITUENT METAL POWERS ARE PRODUCED WITH A FINE LAMELLAR-LIKE STRUCTURE WITH THE OXIDE PARTICLES UNIFORMLY DISTRIBUTED ALONG THE WELD INTERFACES (FIG. 30).

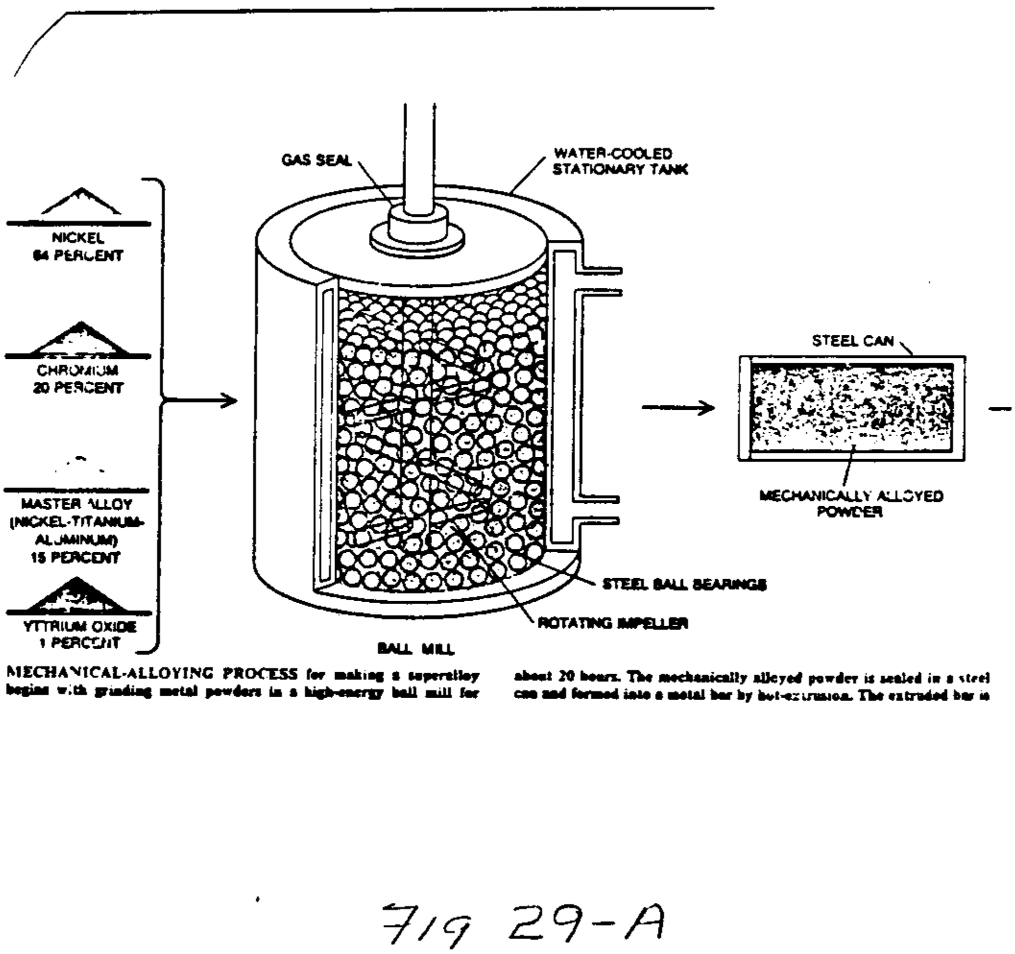

MECHANICAL-ALLOYING PROCESS for making a superalloy begins with grinding metal powders in a high-energy ball mill for about 20 hours. The mechanically alloyed powder is sealed in a steel can and formed into a metal bar by hot-extrusion. The extruded bar is

Fig 29-A

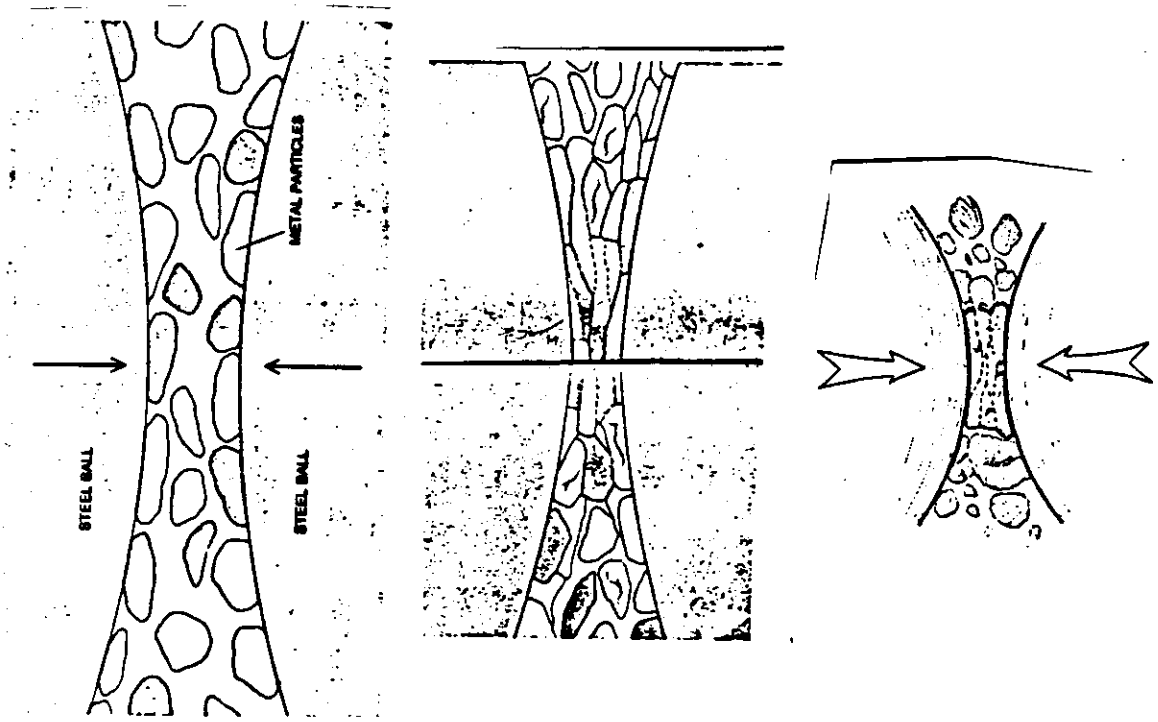

Fig 29-B

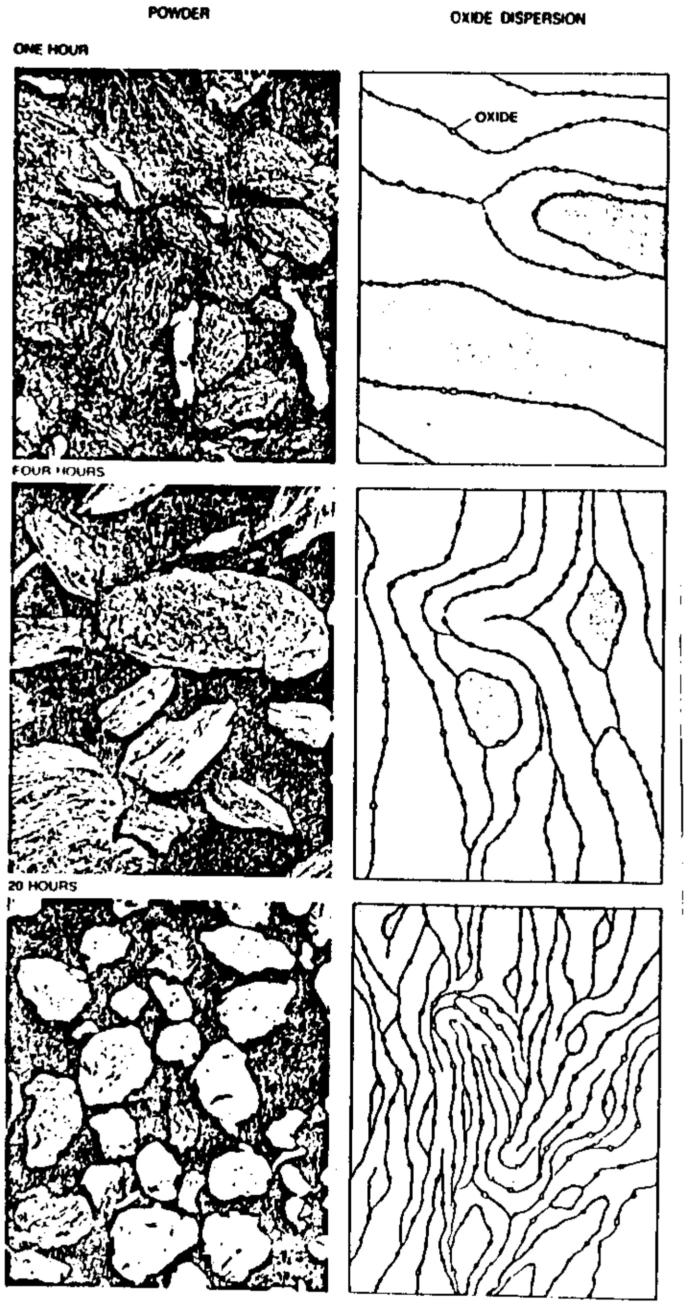

Fig 30

- THE POWERS ARE THEN CONSOLIDATED BY EXTRUSION OR HOT ISOSTATIC PRESSING (HIP). CONSOLIDATED PIECES ARE THEN SUBJECTED TO HOT AND/OR COLD DEFORMATION PROCESSING UNDER CONDITIONS WHICH LEAVE THEM WITH A HIGH LEVEL OF STORED ENERGY. MATERIAL MUST THEN BE IN SUCH A STATE IN ORDER TO DEVELOP COARSE, ANISOTROPIC GRAINS DURING A SUBSEQUENT RECRYSTALLIZATION HEAT TREATMENT (E.G. ZONE ANNEALING PROCESS) (FIG. 31).

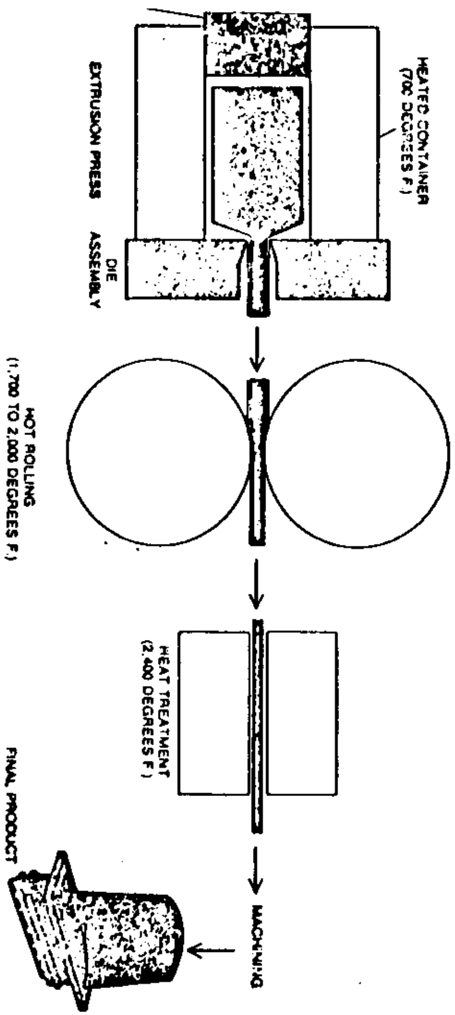

Fig 31

STRUCTURE AND PROPERTIES OF MA ODS ALLOYS

- TABLE 11 LISTS THE COMPOSITIONS OF MA ALLOYS DEVELOPED BY INCO.

- THE MICROSTRUCTURE OF MA-6000E AFTER ZONE RECRYSTALLIZATION AND HEAT TREATMENT IS ILLUSTRATED IN FIG. 32. HEAT TREATMENT: 1/2 H/1232°C/AC + 2 H/954°C/AC + 24 H/843°C/AC STRUCTURE FEATURE: √

  VOLUME PERCENT OF OXIDE: 2.5%

  γ' PARTICLE SIZE: 350 Å

  VOLUME PERCENT OF γ': 50 ~ 55%

- STRENGTHENING MECHANISMS: AT LOW TEMPERATURES, γ' HARDENING IS ACHIEVED; AND ABOVE 1000°C THE STRENGTH IS PROVIDED BY DISPERSION OF OXIDE.

- CREEP PROPERTIES

  FIG. 33—COMPARISON OF STRESS RUPTURE PROPERTIES OF MA-6000E WITH SEVERAL OTHER SUPERALLOYS. MA-6000E IS STRONGER THAN D.S. MAR-M-200 + Hf AT TEMPERATURES ABOVE 870°C.

  FIG. 34—CREEP RUPTURE PROPERTIES OF Fe-BASE ALLOY MA-956, AND Ni-BASE ALLOYS MA-754 AND 757. THE MA ALLOYS ARE MUCH MORE RESISTANT IN CREEP THAN INCONEL ALLOYS.

Nominal Compositions of Mechanical Alloys, wt %

Alloy	Cr	Y_2O_3	Al	Ti	C	Fe	Ta	Mo	W	Ni	Zr	B
Inconel MA754	20	0.6	0.3	0.5	0.05					Bal*		
Incoloy MA956E	20	0.5	4.5	0.5		Bal*						
MA6000E	15	1.1	4.5	2.5			2.0	2.0	4.0	Bal*	0.1	0.01

* Bal = balance.

Table II


(a)
(b)

Figure Micrographs illustrating (a) the grain morphology and (b) the uniform oxide and γ' dispersion in MA 6000E.

Fig 32

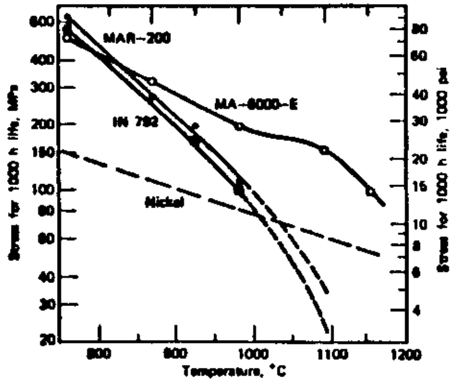

Stress for 1000-h life as a function of temperature in MA-6000-E, DS MAR-M-200 + Hf, IN-792, and TD-Nickel (33). Courtesy of the Metallurgical Society of AIME.

719 33

66

RAPID SOLIDIFICATION RATE PROCESSING AND APPLICATION TO SUPERALLOYS

- ONE OF THE NEW TECHNIQUES FOR THE PROCESSING OF SUPERALLOYS WHICH HAS BEEN EXPLORED WITH INCREASING ENTHUSIASM IN THE PAST YEARS IS THE USE OF RAPIDLY SOLIDIFIED POWDERS IN THE FABRICATION OF SUPERALLOY COMPONENTS.

- FUNDING FOR RS SUPERALLOYS: $9 MILLION FOR 1981

  $11 MILLION FOR 1982

  MAJOR SUPPORTS ARE BEING PROVIDED BY DOE, NASA, AND DOD

ADVANTAGES OF RS MATERIALS

IN GENERAL

- MINIMIZE CHEMICAL SEGREGATION DURING SOLIDIFICATION
- ELIMINATE THE FORMATION OF MASSIVE PHASES (E.G. EUTECTICS)
- INCREASE THE SOLUBILITY OF ALLOYING ELEMENTS (EXTENSION OF SOLID SOLUBILITY LIMIT)
- MICROSTRUCTURAL REFINEMENT
- RETAIN METASTABLE PHASES

FOR RS SUPERALLOYS

- EXCELLENT ALLOY HOMOGENEITY
- INCREASE IN INCIPIENT MELTING POINT
- DIRECTIONAL RECRYSTALLIZATION FOR ORIENTED GRAINS
- CREEP AND STRESS RUPTURE IMPROVEMENTS
- INCREASED OXIDATION RESISTANCE
- INCREASED HOT CORROSION RESISTANCE

7/9 37

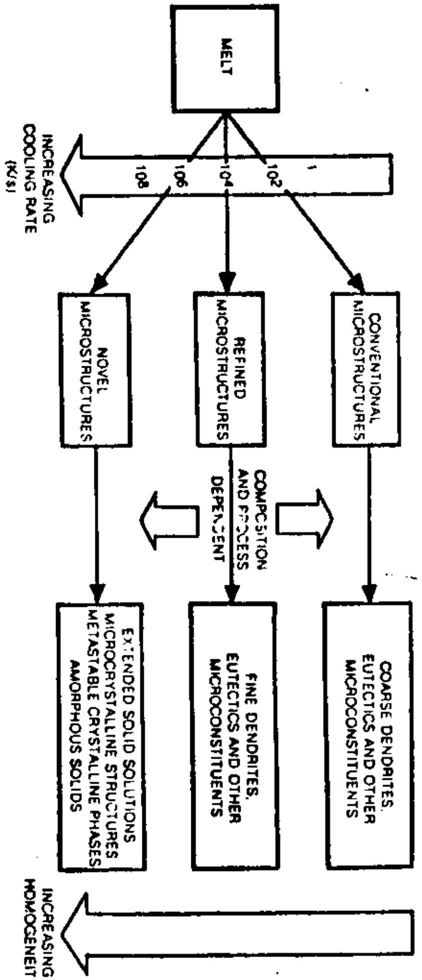

COOLING RATE DEPENDENCE OF SOLIDIFICATION MICROSTRUCTURES

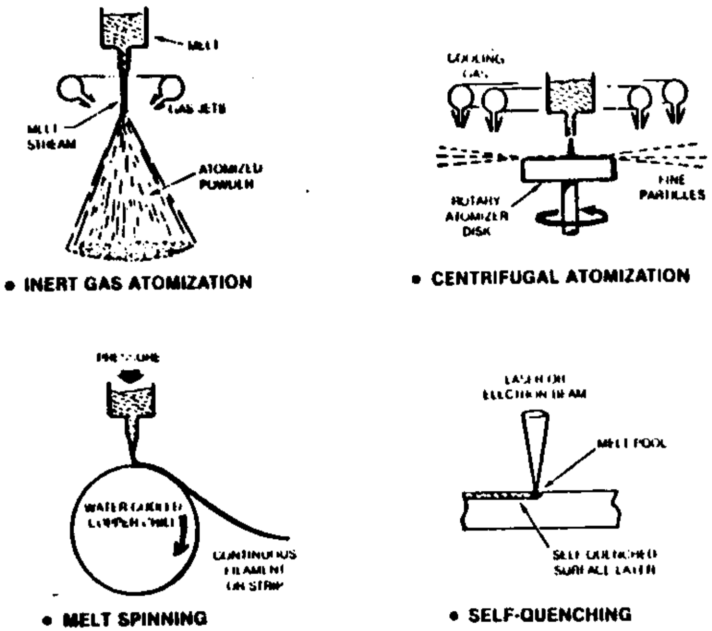

EXAMPLES OF RAPID SOLIDIFICATION METHODS

70

Fig 38

Laser Spin Atomization Device

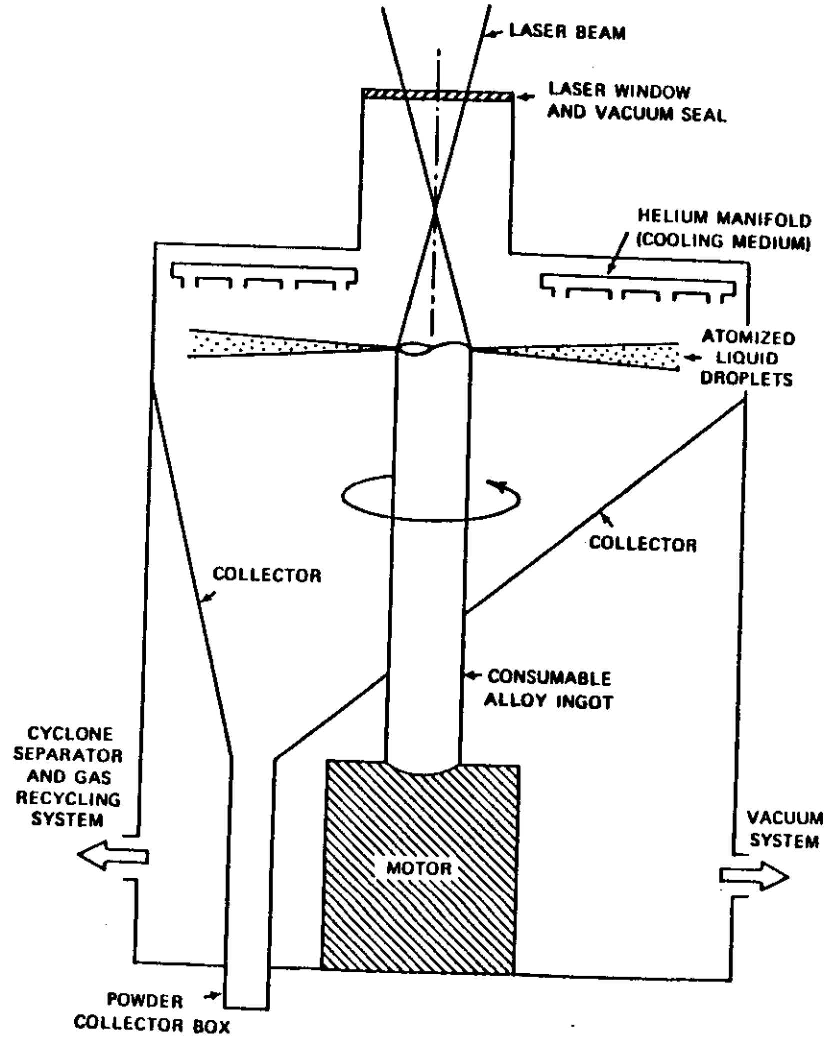

71

Fig 39

EXPERIMENTAL RSR POWDER-PROCESSED DEVICE

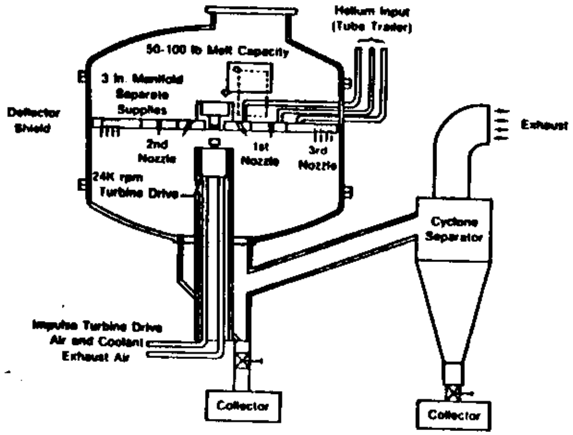

72
7/9 40

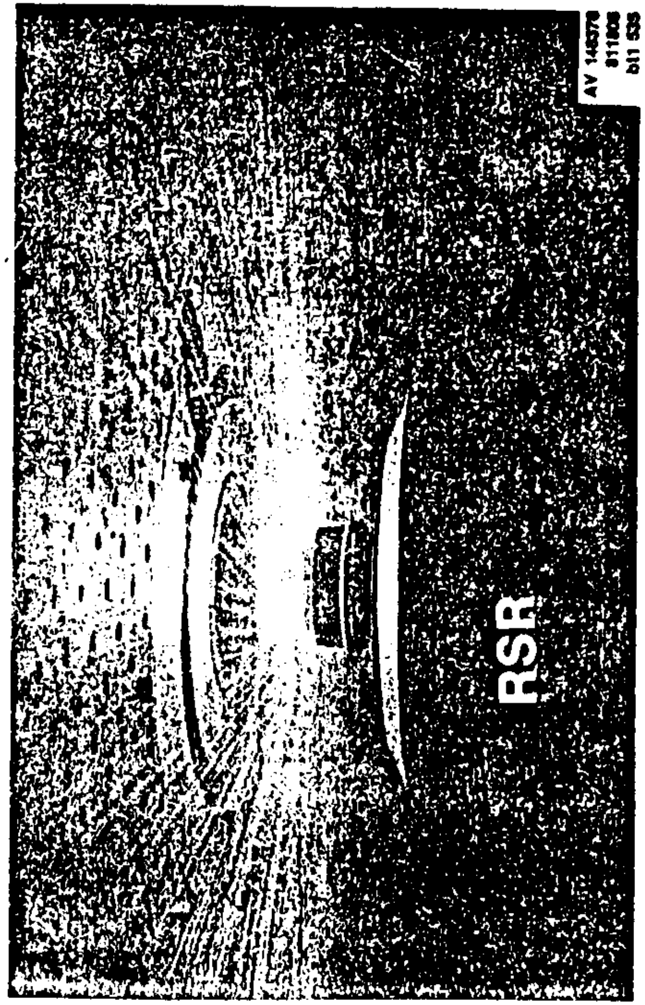

REVOLUTIONARY POWDER METALLURGY OFFERS
NEW DIMENSION FOR SUPERALLOY DEVELOPMENT

7/9 41

73

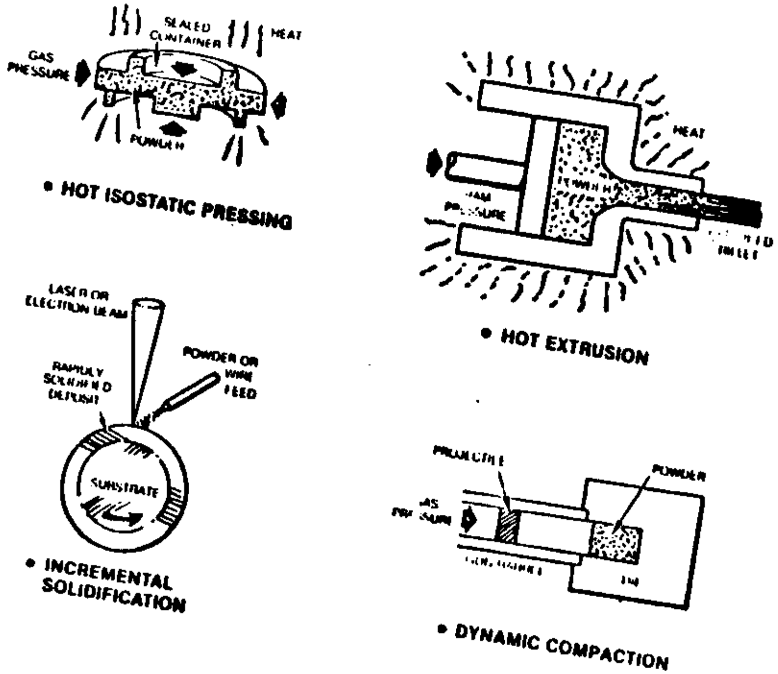

CONSOLIDATION METHODS

719 42

INCIPIENT MELTING POINT OF RSR POWDER-PROCESSED ALLOYS VS CAST ALLOYS

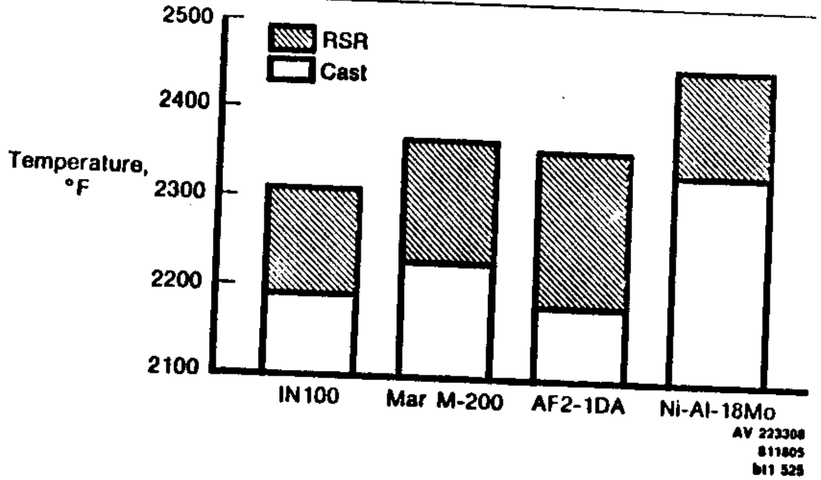

719 43

CREEP RESISTANCE OF SUPERALLOYS

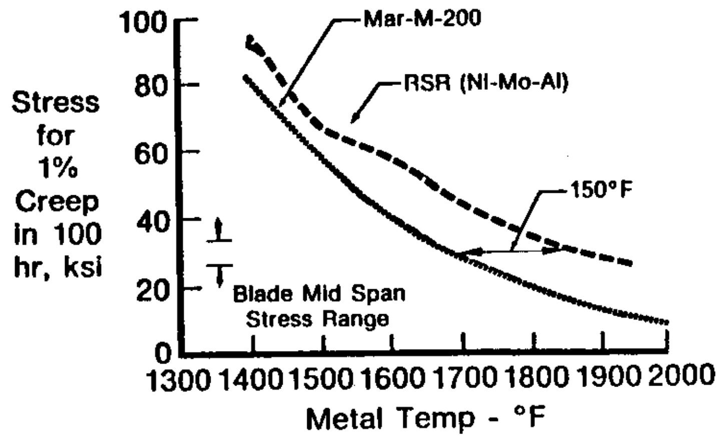

719 45

46

RADIAL WAFER BLADE CONSTRUCTION

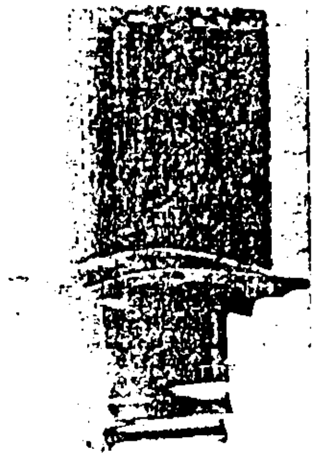

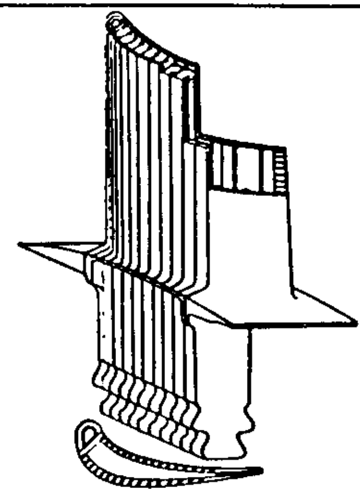

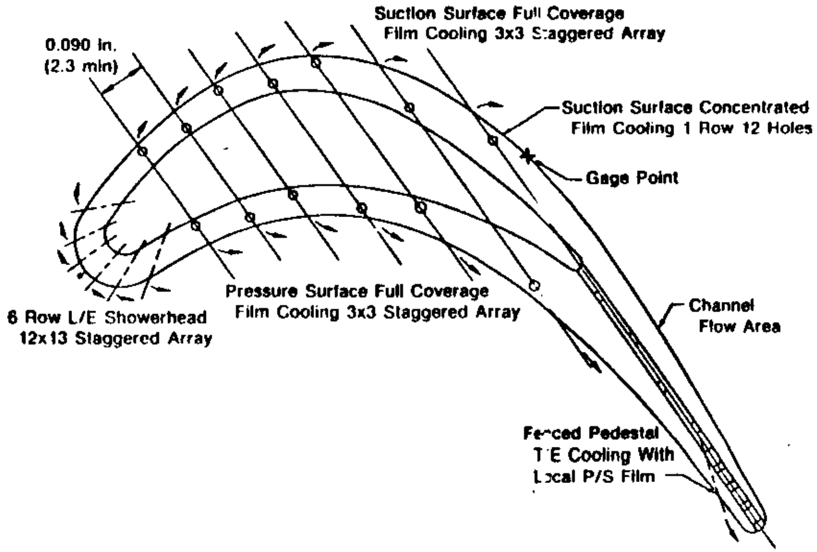

719 50

47

RAPIDLY SOLIDIFIED SUPERALLOYS — EXPECTED RESULTS

- HIGHER PERFORMANCE STRUCTURAL MATERIALS
- CHEAPER TO FABRICATE
- LESS DEPENDENT ON STRATEGIC/CRITICAL ELEMENTS
- VASTLY IMPROVED COMPONENT DURABILITY
- UTILIZE ADVANCED DESIGN TECHNIQUES

DIRECTIONALLY SOLIDIFIED EUTECTIC COMPOSITES

(ALIGNED EUTECTIC ALLOYS)

- D.S. TECHNIQUES ARE COMMONLY USED TO PRODUCE WELL ALIGNED FIBERS AND LAMELLAE AT CONTROLLED GROWTH RATES.
- ALIGNED EUTECTICS HAVE OUTSTANDING MECHANICAL PROPERTIES AT HIGH TEMPERATURES (800–1150°C), DUE TO STRENGTHENING BY ALIGNED FIBERS OR LAMELLAE.
- POTENTIAL TO BE USED AS GAS TURBINE MATERIALS AT TEMPERATURES ABOVE 900°C.
- MECHANICAL PROPERTIES OF ALIGNED EUTECTICS DEPEND ON THE INTERPHASE SPACING (λ) WHICH CAN BE REFINED THROUGH INCREASING GROWTH RATE (R)

$$\lambda^2 R = \text{CONST.}$$

- THE YIELD AND FLOW BEHAVIOR OF ALIGNED EUTECTICS CAN BE GENERALLY EXPRESSED BY THE EQS.

$$\sigma_f = \sigma_i + K\lambda^{-1/2}, \text{ OR}$$

$$\sigma_f = \sigma_i + K_1 R^{1/4}$$

SYSTEM AND COMPOSITION OF ALIGNED EUTECTICS

• SYSTEM	MORPHOLOGY
$\gamma - \alpha$ (Mo,W)	FIBER
$\gamma/\gamma' - \alpha$	FIBER
$\gamma - \delta$ (E.G. Ni_3Nb)	LAMELLAE
$\gamma/\gamma' - \delta$	LAMELLAE
$\gamma' - \delta$ ($Ni_3Al - Ni_3Ta$)	LAMELLAE
γ – CARBIDE (E.G. TaC,NbC)	FIBER
γ/γ' – CARBIDE	FIBER

- HIGH-TEMPERATURE EUTECTIC ALLOY COMPOSITION IS LISTED IN TABLE 13.

- TYPICAL MICROSTRUCTURES OF ALIGNED EUTECTICS

  FIG. 61: $\gamma/\gamma' - \delta$ (Ni_3Nb)

  γ – CARBIDE (TaC)

  $\gamma'/\gamma - \alpha$ (Mo)

TABLE High temperature eutectic alloy composition

Alloy	Morphology	V_f	Ni	Co	Cr	Al	Nb	Mo	Ta	C	Other
						w% Solute					
Nitac	F	0.05	69	-	10	5	-	-	14.9	1.1	-
Nitac 13	F	-	63	3.3	4.4	5.4	-	-	8.1	0.54	3.1W, 6.2Re, 5.6V
Cotac 74	F	-	bal	20	10	4	4.9	-	-	0.55	10W
Cotac 741	F	-	bal	10	10	5	4.7	-	-	0.6	10W
Cotac	F	0.10	10	65	10	-	-	-	14	1	-
Cotac 3 or 33*	F	0.10	10	56	20	-	-	-	13	1	-
Cotac 5083W	F	0.10	9.5	59	16.7	-	-	-	12	0.77	3W
γ/γ'-δ (6%Cr)	L	0.37	71.5	-	6	2.5	20	-	-	-	-
γ/γ'-δ (0%Cr)	L	0.3	76.5	-	-	2.5	21	-	-	-	-
γ'/γ-Mo (AG-15)	F	0.26	66.5	-	-	5.1	-	28.4	-	-	-
γ'/γ-Mo (AG-34)	F	0.26	62.5	-	-	6.3	-	31.2	-	-	-
γ-δ	L	0.26	76.7	-	-	-	23.3	-	-	-	-
Ni_3Ta-Ni_3Al	L	0.35	64.1	-	-	4.9	-	-	31	-	-
Co,Cr-$(Co,Cr)_7C_3$	F	0.30	-	56.6	41	-	-	-	-	2.4	-
γ/γ'-Ni_3Ta	L	-	67.6	-	-	3.7	-	-	28.7	-	-
Ni-Ni_3Ta	L	-	63	-	-	-	-	-	37	-	-
γ'-δ	L	0.44	bal	-	-	4.4	23.4	-	-	-	-
Co,Cr-$(Cr$-$Co)_7C_3$	F	0.3	-	bal	41	-	-	-	-	2.4	-

* 1300°C, 2 hr; 1000°C, 24 hr, A.C.

Table 13

(a)

. Transverse microstructures of several high temperature eutectic composites:
a) γ/γ'-δ (0%Cr), R = 3 cm/hr

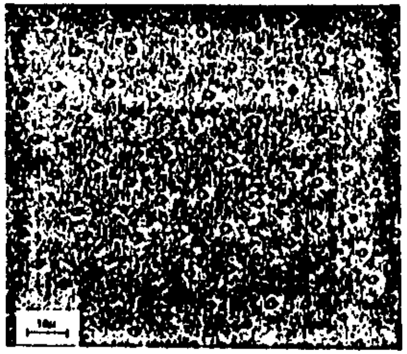

(e)

f) Ni, 10Cr, 5Al-TaC, R = 0.6 cm/hr

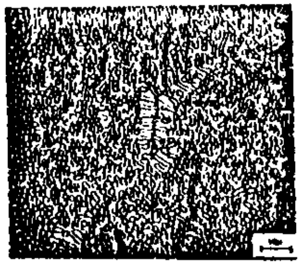

(d)

. (cont).
b) γ/γ'-δ (6%Cr), R = 3 cm/hr
c) Co, 10Cr, 10Ni-TaC, R = 2.6 cm/hr
d) γ'/γ-Mo (AG-15) R = 1.9 cm/hr

719 61

TENSILE PROPERTIES OF ALIGNED EUTECTICS

- STRENGTHENING MECHANISMS: SS + PRECIPITATION OF γ' AND CARBIDES + FIBER/LAMELLAE
- LONGITUDINAL TENSILE PROPERTIES OF AS-GROWN ALIGNED EUTECTICS, 25°C (TABLE 14)
- EFFECT OF TEMPERATURE ON ULTIMATE TENSILE STRENGTH OF HT EUTECTICS (FIG. 62)
  - —Cotac 74 IS THE STRONGEST ALLOY AT RT
  - —Nitac 13 EXHIBITS THE HIGHEST STRENGTH ABOVE 800°C
  - —MOST EUTECTICS IN THIS FIGURE ARE STRONGER THAN THE CONVENTIONAL SUPERALLOYS SUCH AS IN-100 ABOVE 1000°C
- EFFECT OF λ ON YIELD AND TENSILE STRENGTHS OF $\gamma' - \delta$ AT 1093°C (FIG. 63) $\sigma = \sigma_i + K\lambda^{-1/2}$
- EFFECT OF TEMPERATURE AND HEAT TREATMENT ON TENSILE PROPERTIES OF $\gamma/\gamma' - \delta$ (FIG. 64)
- OFF-AXIS PROPERTIES: OFF-AXIS PROPERTIES OF COMPOSITES ARE INFERIOR TO THOSE OF THE LONGITUDINAL ORIENTATION
  - FIG. 65: COMPARISON OF TRANSVERSE AND LONGITUDINAL TENSILE STRENGTH OF SEVERAL HT EUTECTICS
  - FIG. 66: TEMPERATURE DEPENDENCE OF LONGITUDINAL AND TRANSVERSE STRENGTH AND DUCTILITY OF $\gamma/\gamma' - \delta$ (6% Cr)

Longitudinal tensile properties of as-grown aligned eutectics, 25°C

Alloy**	Type	T_m °C	ρ g/cc	R cm/hr	σ_y MN/m²	σ_y ksi	σ_{UTS} MN/m²	σ_{UTS} ksi	% Elong.	Ref.
Nitac	D–B	1348	~8.8	0.6	814*	118*	1304	189	54	32
Nitac 13	D–B	-	-	0.6	-	-	1420	206	-	14
Cotac 74	D–B	1336	8.6	-	1260*	182.8*	1550	225	12.4	59
Cotac (Co,Cr,Ni-TaC)	D–B	1402	9.0	0.8	787*	114*	963	139.5	30	31
Cotac (Co,Cr,Ni-TaC)	D–B	1402	9.0	2.5	842*	122*	1042	151	33	32
γ/γ'-δ (0%Cr)	D–SB	1272-1274	-	3	814	118	1193	173	~30	32
γ/γ'-δ (6%Cr)	D–SB	1244-1257	8.6	3	648	94	1187	172	3.0	32
γ'/γ-Mo (AG-15)	D–D	1306	8.2	1.9	621	90	1346	195	21.9	71
γ'/γ-Mo (AG-34)	D–D	-	-	0.76	580	84	1446	209.8	19.2	71
γ'-δ	D–SB	1280	8.5		1035	150	1242	180	< 1	6
γ-δ	D–SB	1270	-	0.6-4.8	428	62	863	125	22	72
Co,Cr-(Co,Cr)$_7$C$_3$	D–B	1330	8.0		828	120	1380	200	< 2	73
Ni$_3$Ta-Ni$_3$Al	B–D	~1360	-	1.33	690	100	725	105	< 1	74
γ/γ'-Ni$_3$Ta	D–B	~1360	-	1.33	916	132.9	984	142.7	2.8	23
γ-Ni$_3$Ta	D–B	1360	11.1	0.5	962	139.4	962	139.4	-	75

* fiber fracture stress (upper yield stress)

** matrix phase listed first.

Table 14

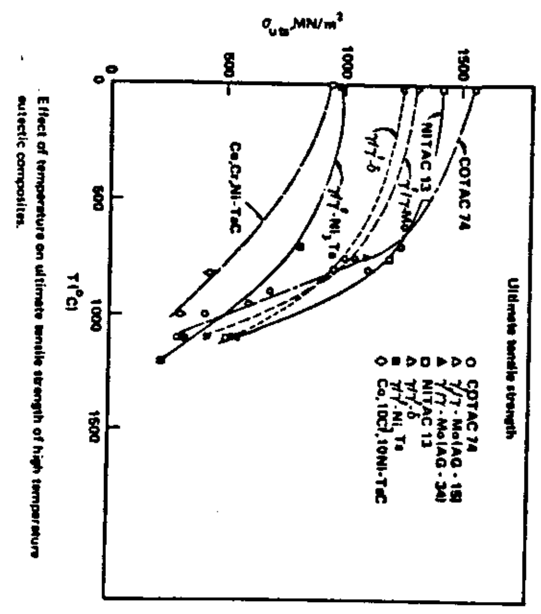

. Effect of temperature on ultimate tensile strength of high temperature eutectic composites.

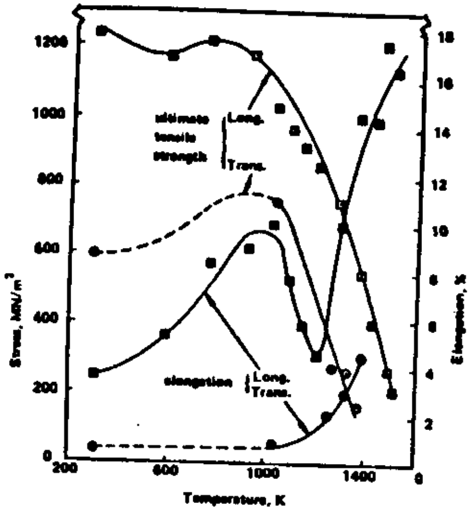

Temperature dependence of longitudinal and transverse strength and ductility of γ/γ'-δ (8%Cr) /17/.

Fig 66

CREEP PROPERTIES OF ALIGNED EUTECTICS

- EXCELLENT CREEP STRENGTH AT HT (FIGS. 67 AND 68)

  THE CREEP RESISTANCE OF ALIGNED EUTECTICS IS SUPERIOR TO COMMERCIAL SUPERALLOYS AT HT

- $\dot{\varepsilon}$ CAN BE GENERALLY EXPRESSED BY THE EQUATION

$$\dot{\varepsilon} = A\sigma^{n}e^{-Q/RT}$$

  THE CREEP PARAMETERS ARE GIVEN IN TABLE 14

- RECENT WORK HAS SHOWN THAT DECREASING λ OR FIBER RADIUS
  - —RESULTS IN GREATLY ENHANCED CREEP RESISTANCE FOR SEVERAL ALLOYS (FIG. 69)
  - —THE BENEFICIAL ASPECTS OF INCREASING R TO REFINE λ CONTINUES SO LONG AS STRUCTURE IS WELL ALIGNED. CELLULAR MICROSTRUCTURES OBTAINED AT HIGH R LEAD TO INFERIOR STRESS-RUPTURE PROPERTIES

- CREEP PROPERTIES TEND TO BE LESS ATTRACTIVE WHEN TESTED IN AN OFF-AXIS DIRECTION (FIG. 70)

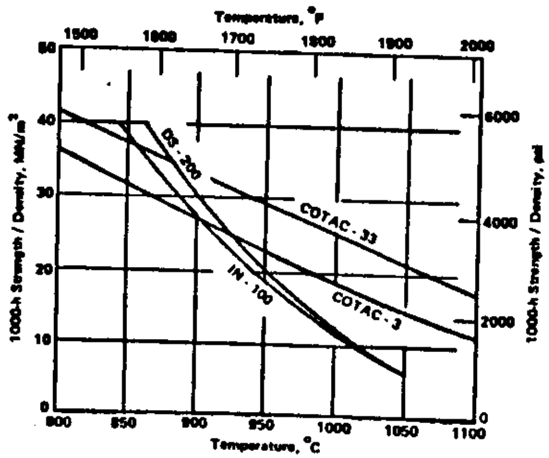

. Comparison of specific 1000 hr. rupture strength of Cotac 33 (heat treated to precipitate carbides) with Cotac 3 and two nickel-base superalloys /30/.

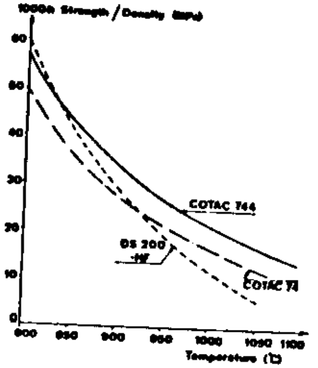

Specific 1000-hour rupture strength vs. temperature curves for Cotac 744, Cotac 74 and DS200 Hf.

719 67

719 68

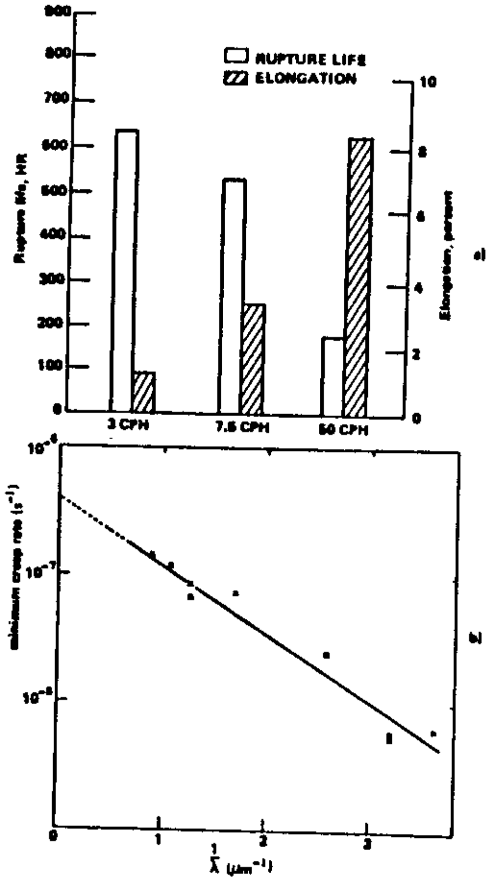

Fig. 11. Effect of solidification rate (interfiber spacing or fiber radius) on creep-rupture properties at 980°C.
a) rupture life and elongation of γ/γ'-δ (6%Cr) /28/
b) minimum creep rate of γ/γ'-Cr_3C_2 vs. fiber radius, λ /28/.

LENGTH MEMORY EFFECT OF ALIGNED EUTECTICS

- A UNIQUE FEATURE OF SOME EUTECTICS IS THAT HEAT TREATMENTS AFTER CREEP, NOT ONLY PERMIT THE RESTORATION OF THEIR CREEP STRENGTH BUT ALSO ALLOW THE RECOVERY OF THEIR INITIAL LENGTH.

- EXPERIMENTAL OBSERVATION OF THE LENGTH MEMORY EFFECT IN Cotac 744 (Ni-10 Co-4 Cr-10 W-2 Mo-6 Al-3.8 Nb-0.47 C)
  - –PERFORM CREEP TESTS (OR TENSILE TESTS) TO 1.5% PRIOR TO THE ONSET OF TERTIARY CREEP
  - –REMOVE THE CREEP LOAD AND HEAT TREAT FOR 20 MIN/1200°C/AC + 16 H/850°C/AC
  - –SPECIMENS CONTRACT TO NEARLY THEIR INITIAL LENGTH.

- THE PERIODIC HEAT TREATMENTS IMPROVE CREEP RUPTURE LIFE, DUE TO THE LENGTH MEMORY EFFECT (TABLE 15).

- THERMAL EXPANSION MISMATCH BETWEEN PHASES OF SOME D.S. EUTECTICS (TABLE 16).

- THE LENGTH MEMORY EFFECTS IS BELIEVED TO BE DUE TO THE THERMAL EXPANSION MISMATCH BETWEEN PHASES OF D.S. EUTECTICS
  - –WHEN THE COMPOSITE IS SUBJECTED TO A PLASTIC DEFORMATION, IN TENSION, THE FIBERS DEFORM ELASTICALLY AND THE MATRIX DOES PLASTICALLY
  - –IF THIS STRAINED IS NOW HEATED TO A SUFFICIENTLY HT (~1200°C) IN THE ABSENCE OF AN EXTERNAL STRESS, THE ELASTIC FIBERS WILL EXERT A COMPRESSION STRESS ON THE PLASTIC MATRIX SO THE BACKWARD FLOW OCCURS

Improved stress-rupture lives due to "length memory effect".

Creep tests		Length measurements (mm)					Time (hours)	
temperature (°C)	stress (MPa)	initial length	after 1st creep	after heat treatment	after 2nd creep	after heat treatment	total time to rupture	uninterrupted tests
850	400	30.02	30.40	30.06	30.42	30.10	1040	700*
900	210	29.98	30.36	30.08	30.39	30.06	1303	700*

* Average of three tests

. Approximate thermal expansion mismatch between phases of some D.S. eutectics /18/

D.S. Eutectic	Average Thermal Expansion Mismatch (°C)
Ni-NbC	10.0×10^{-6}
Ni,Cr-NbC	9.4×10^{-6}
Co,Cr-NbC	9.4×10^{-6}
Co,Cr,Ni-TaC	9.9×10^{-6}
Ni,Cr-TaC	9.9×10^{-6}
Ni,Cr,Al-TaC	8.1×10^{-6}
Ni_3Al-Ni_3Nb $(\gamma'$-$\delta)$	1.6×10^{-6}
(Ni,Cr) (Ni_3Al)-Ni_3Nb, $(\gamma/\gamma'$-$\delta)$	6.1×10^{-6}

—THIS TYPE OF REVERSED FLOW SHOULD BE EXPECTED IN MANY D.S. EUTECTICS HAVING A ELASTIC FIBRUS AND A PLASTIC MATRIX.

- FROM A TECHNOLOGICAL STANDPOINT, THIS PHENOMENON IS OF GREAT INTEREST TO THE ENGINE MANUFACTOR.